# A Positive Low Cloud–Sea Surface Temperature Feedback in the East Asian Marginal Seas during El Niño Mature Winters and Their Following Spring

ZHUN GUO,[a] KALLI FURTADO,[b] TIANJUN ZHOU,[c] VINCENT E. LARSON,[d,e] AND LING ZHANG[f]

[a] *Climate Change Research Center, Institute of Atmospheric Physics, Chinese Academy of Sciences, Beijing, China*
[b] *Met Office, Exeter, United Kingdom*
[c] *LASG, Institute of Atmospheric Physics, Chinese Academy of Sciences, Beijing, China*
[d] *Department of Mathematical Sciences, University of Wisconsin–Milwaukee, Milwaukee, Wisconsin*
[e] *Pacific Northwest National Laboratory, Richland, Washington*
[f] *School of Atmospheric Physics, Nanjing University of Information Science and Technology, Nanjing, China*

ABSTRACT: During the winter and subsequent spring of an El Niño year, the East Asian marginal sea (EAMS) exhibits positive sea surface temperature anomalies (SSTAs) and fewer low clouds, while the western North Pacific experiences negative SSTAs. In this study, we suggest that the positive SSTAs in EAMS are maintained by a positive low cloud–SST feedback. In neutral winters and springs, the EAMS is covered by low clouds, which have a cooling effect on surface temperatures. During an El Niño year, a western North Pacific anomalous anticyclone is established, and along its northwestern flank, there are favorable conditions for convergence of moisture and weaker surface latent heat flux over the EAMS. Once a positive SSTA has been established, a further reduction of turbulent mixing results in less low cloud and enhanced solar heating of the ocean mixed layer; this reinforces and maintains both the positive SSTA and the lack of low cloud via a positive feedback mechanism. The concurrent increase of low cloud–SST feedback and anticyclone circulation strengths is evident in the coupled-model simulations from phase 6 of the Coupled Model Intercomparison Project. Furthermore, sensitivity experiments, performed with the atmospheric components of Community Earth System Model (CESM2), reveal that a positive SSTA helps to maintain the western North Pacific anomalous anticyclone. Four pacemaker-coupled experiments by CESM2, with sea surface temperature in the equatorial Pacific restored to the observational anomalies plus the model climatology and altered low cloud feedback over EAMS, suggest that the low cloud–SST feedback results in more than the maintenance of a positive SSTA over the EAMS: the positive feedback is also a previously overlooked mechanism for the maintenance of the western North Pacific anomalous anticyclone.

SIGNIFICANCE STATEMENT: The East Asian marginal sea (EAMS) and western North Pacific are important areas that bridge El Niño and the climate of East Asia. Unlike the cold sea surface temperature anomaly (SSTA) over the western North Pacific during El Niño, the positive SSTA over EAMS, which is covered by winter low cloud, has received less attention. We suggest that a "low cloud–SST" feedback—namely, one in which decreasing low-level clouds allows more sunlight to strike the ocean surface and favors higher SST—maintains the positive SSTA over EAMS. We also configure a widely used atmospheric model with a set of preset SSTA patterns that mimic different climate patterns. Our experiments with different climate patterns and CMIP6 historical runs show that the low cloud–SST feedback (through the positive SSTA) is a possible supplementary mechanism for reinforcing the WNP anomalous anticyclone.

KEYWORDS: Asia; Atmosphere-ocean interaction; Cloud cover; Clouds; Feedback; Climate models

## 1. Introduction

In the western North Pacific (WNP), an anomalous lower-tropospheric anticyclone (WNPac), which is coupled to a negative sea surface temperature anomaly (SSTA), provides a link between El Niño–Southern Oscillation (ENSO) events in the eastern-tropical Pacific and the East Asian monsoon (Wang et al. 2000; Zhang et al. 1996). It is widely accepted that the WNPac matures in El Niño winter and then persists during the following spring and summer. But there is no widespread agreement about the mechanisms that maintain the WNPac.

One of the views emphasizes the local air–sea interactions over the western North Pacific. For example, previous studies have suggested that the positive "wind–evaporation–SST" feedback is essential to the maintenance of the SSTA, which can persist until the following spring or early summer (Wang et al. 2000, 2003). In this framework, the SSTA forms in autumn or winter in response to atmospheric Rossby waves that are generated by El Niño–induced subsidence over the equatorial western Pacific. But these cold anomalies may "out live" the El Niño events themselves (by several months, in extreme cases) because the anomalous southwesterlies (northeasterlies) on the western (eastern) flanks of the WNPac, strengthen (weaken) the climatological northeasterly trade winds and latent heat fluxes that act to maintain a gradient of negative/positive SSTA across the anticyclone.

An alternative view favors the remote effects of El Niño SSTA over the eastern Pacific and the interactions between El Niño and the annual cycle over local air–sea interactions.

*Corresponding author*: Zhun Guo, guozhun@lasg.iap.ac.cn

Based on the sensitivity experiments of an atmospheric general circulation model, Stuecker et al. (2015) found that WNPac is well established and maintained under the forcing of the eastern tropical Pacific SSTAs, indicating that the air–sea interaction in the northwestern Pacific is secondary for WNPac. Some more recent studies also emphasize the remote effects of El Niño SSTA over the eastern Pacific in maintaining WNPac during El Niño mature winter and the following spring, based on the observational moist static energy budgets and a series of "pacemaker-coupled" experiments (Wu et al. 2017a,b). Pacemaker-coupled experiments are fully coupled simulations except that the sea surface temperature (SST) in the equatorial Pacific is restored to the observational anomalies plus the model climatology. They further quantified the relative contributions of remote SSTA forcing and local air–sea interactions to the intensity of the WNPac and found that the former dominates, because the northern branch of the twin cyclonic responses advects dry and low moist enthalpy air into WNP and suppresses local convections.

In the view of remote effects of SSTAs, previous studies (Xie et al. 2009; Yang et al. 2007) also highlighted the warming effect from the Indian Ocean. The Indian Ocean warming acts like a capacitor that helps to prolong the effects of El Niño after the SSTAs diminish in the tropical eastern Pacific. Through the moist adiabatic adjustments of local deep convections, the Indian Ocean warming changes the atmospheric heating and emanates the Kelvin wave into the Pacific, which further enhances the WNPac.

These two general kinds of perspectives complement each other, suggesting that WNPac is the result of both the remote forcing and the local air–sea interactions over WNP. Is "low cloud–SST" feedback, as a type of local sea–air interaction, a possible mechanism for maintaining the WNPac? Previous studies showed that the largest annual mean cloud optical depths at the midlatitudes, occur downstream of the Tibetan Plateau, downstream of the East Asian landmass and sea, because of the prevailing low clouds (Klein and Hartmann 1993; Wood 2012; Yu et al. 2004). The large low cloud fraction belt, mainly the stratiform low cloud, extends from southeastern China eastward, to the East Asian marginal sea (EAMS) and then to the North Pacific (Fig. 1). Although there have been many studies of low cloud feedback in the subtropical eastern Pacific (Bony et al. 2006; Bony and Dufresne 2005; Bony et al. 1997; Clement et al. 2009; Norris 2000; Norris and Leovy 1994), the effects of low clouds and their feedback on the interannual variability of SSTs over the EAMS remains unclear. Considering that the EAMS is also one of the low cloud areas and exhibits significant interannual variabilities, we are motivated to investigate low cloud feedbacks and their climate effects. Moreover, formations of prevailing low clouds are known to rely heavily on large-scale controls, such as trade winds and lower-troposphere stability (LTS) (Klein and Hartmann 1993; Wood 2012). So the strong interactions between low clouds and large-scale circulations in WNP may be also expected to occur.

In this study, therefore, we aim to answer two questions: Is there a low cloud feedback over EAMS? If so, how does it play a role in the maintenance of WNPac during El Niño mature winter and the following spring? The remainder of the paper is organized as follows. The data and analysis method are described in section 2. The results are presented in section 3. Section 4 summarizes the major findings.

## 2. Data, method descriptions, and experiment design

### a. Data descriptions

The observational and reanalyzed datasets used in present study consist of: 1) cloud fraction from the International Satellite Cloud Climatology Project (ISCCP) D2 from 1984 to 2007 (Rossow and Schiffer 1999); 2) surface latent flux, sensible flux, longwave and shortwave fluxes by the objectively analyzed air–sea fluxes (OAflux) from 1984 to 2007 (Yu and Weller 2007); 3) the Hadley Centre Sea Ice and Sea Surface Temperature dataset (HadISST) from 1950 to 2015 (Rayner et al. 2003); 4) European Centre for Medium-Range Weather Forecasts interim reanalysis (ERA-Interim; Dee et al. 2011) for circulations and profiles of boundary layer; 5) International Comprehensive Atmosphere–Ocean Dataset (ICOADS; 1° latitude × 1° longitude) that offers observational SST and cloud fraction from ships, buoys, and other platform types from 1950 to 2015 (Woodruff et al. 2008); 6) Global Ocean Data Assimilation System (GODAS) offers the oceanic mixed layer depth, currents, and temperature from 1984 to 2007 (https://www.cpc.ncep.noaa.gov/products/GODAS/background.shtml); and 7) the *Cloud–Aerosol Lidar and Infrared Pathfinder Satellite Observation* (*CALIPSO*) from 2007 to 2017.

The intensity of ENSO events is measured by the DJF-mean Niño-3.4 index, which is defined as the area-averaged SSTA over the region 5°N–5°S, 120°–170°W. Because low-level clouds can be mistakenly identified as midlevel clouds in ISCCP, the low cloud is defined as the sum of midcloud and low cloud (Clement et al. 2009).

To investigate the link between low cloud, SST and large-scale circulations over EAMS, historical experiments during 1850–2015 of 27 fully coupled models from phase 6 of the Coupled Model Intercomparison Project (CMIP6) are analyzed in our study (Table 1).

### b. Diagnostic methods

For analyzing the changes in the marine boundary layer, the entrainment rate $w_e$ is diagnosed from daily ERA-Interim data by following the equation (Zhu et al. 2005):

$$w_e = \frac{dZ_i}{dt} + DZ_i, \tag{1}$$

where the large-scale subsidence rate $DZ_i \approx 0.32$ cm s$^{-1}$ and $Z_i$ is the height of boundary layer. Here, $Z_i$ is defined as the height where the bulk Richardson number (Ri) first exceeds its threshold (Ric) (Holtslag and Boville 1993), namely,

$$Z_i = Z(k+1) + \frac{\mathrm{Ric} - \mathrm{Ri}(k+1)}{\mathrm{Ri}(k) - \mathrm{Ri}(k+1)} \times [Z(k) - Z(k+1)], \tag{2}$$

where $Z$ is height from ERA-Interim, and $k$ is the vertical level index. The Richardson number threshold (Ric) depends on the grid of the dataset (Galperin et al. 2007). Given that

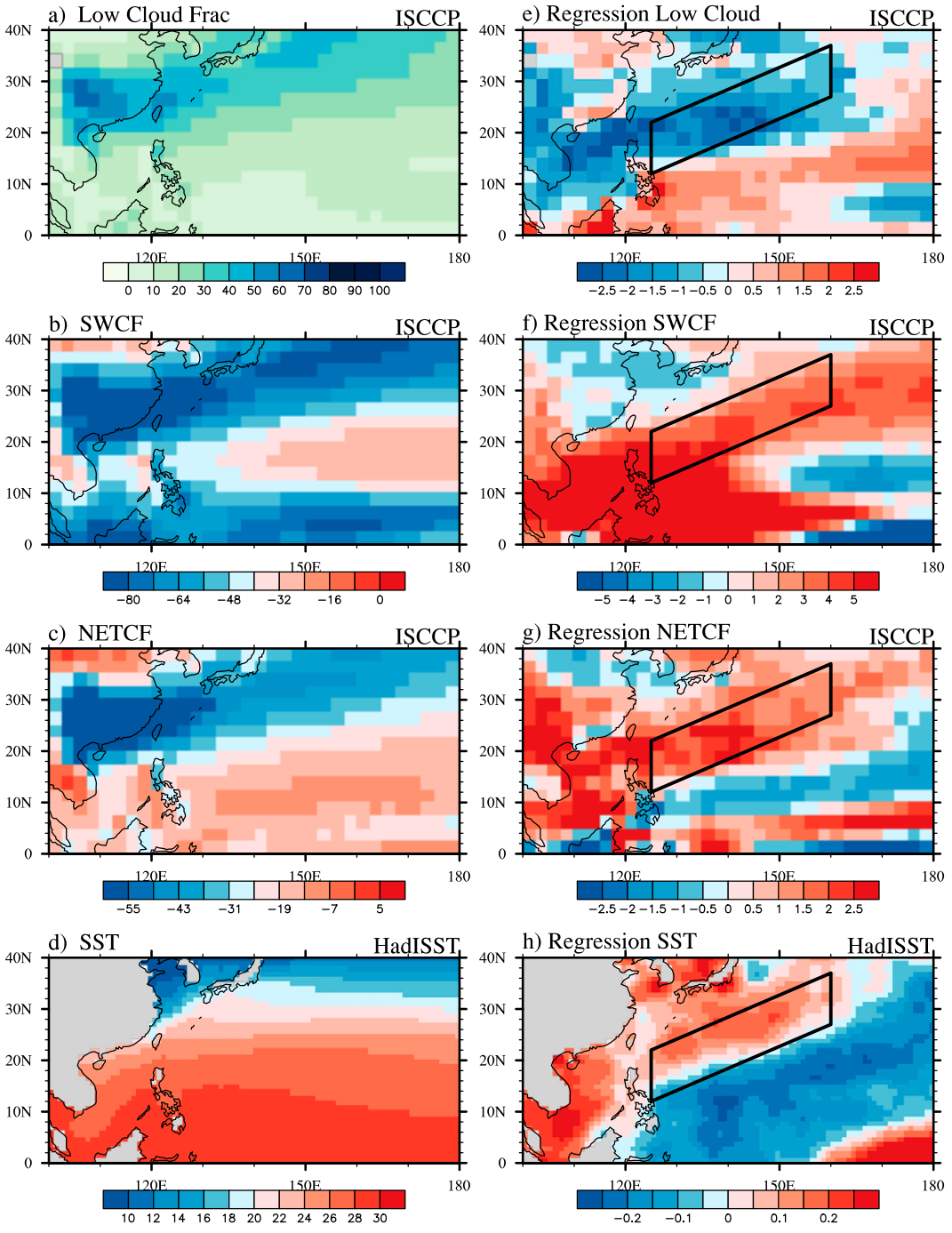


FIG. 1. The climatological DJFMAM mean (a) low cloud fraction (%) from ISCCP D2, (b) SWCF and (c) NETCF from ISCCP FD (W $m^{-2}$), and (d) SST from HadISST (°C). The (e) DJFMAM mean low cloud fraction, (f) SWCF, (g) NETCF from ISCCP, and (h) HadISST SST regressed against the time series of DJF-mean Niño-3.4 index. The black boxes in (e)–(h) are the EAMS, namely, the region is analyzed in later plots and pacemaker experiments. The low cloud fraction, SWCF, and SST build up a positive feedback loop in EAMS.

the vertical resolution of the ERA-Interim (37 levels) is close to that of the Community Earth System Model (CESM2, 32 levels), this study has followed the CESM2's setting that Ric = 0.3.

To better understand the evolution of SSTA over EAMS, the temperature equation of ocean mixed layer is diagnosed in this study. Following Huang et al. (2012, 2010), the SST budget equation is

TABLE 1. Details of the 27 CMIP6 models used in this study.

| Model | Institute/country | Atmospheric resolution (lat × lon, level) | Correlation between SWCF and SST over EAMS (box in Fig. 1) | Vorticity over the domain 5°–30°N, 125°–150°E ($\times 10^{-6}$ s$^{-1}$) | Precipitation anomalies over the domain 2°–15°N, 125°–160°E (mm day$^{-1}$) |
|---|---|---|---|---|---|
| ACCESS-CM2 | Commonwealth Scientific and Industrial Research Organization, Australia | 145 × 192, L85 | 0.17 | −0.29 | −1.75 |
| ACCESS-ESM1–5 | — | 144 × 192, L85 | 0.14 | −0.05 | −0.68 |
| BCC_CSM2-MR | Beijing Climate Center, China | 160 × 320, L46 | −0.26 | −0.01 | −0.78 |
| BCC_ESM1 | — | 64 × 128, L26 | −0.13 | −0.22 | −1.15 |
| CanESM5 | Canadian Centre for Climate Modeling and Analysis, Canada | 64 × 128, L49 | 0.03 | −0.02 | −0.66 |
| CAMS-CSM1–0 | Chinese Academy of Meteorological Sciences, China | 160 × 320, L31 | 0.30 | 0.77 | 0.14 |
| CESM2 | National Center for Atmospheric Research, United States | 192 × 288, L32 | 0.33 | −1.16 | −2.63 |
| CNRM-ESM2–1 | Centre National de Recherches Météorologiques-Centre Européen de Recherche et de Formation Avancée en Calcul Scientifique, France | 128 × 256, L91 | 0.18 | −0.34 | −1.60 |
| CNRM-CM6–1-HR | — | 360 × 720, L91 | 0.03 | −0.18 | −0.87 |
| CNRM-CM6–1 | — | 128 × 256, L91 | 0.19 | −0.36 | −1.41 |
| FGOALS-g3 | Chinese Academy of Sciences, China | 90 × 180, L30 | −0.02 | −0.35 | −1.16 |
| FGOALS-f3-l | — | 218 × 360, L32 | 0.22 | −1.35 | −2.38 |
| GFDL-CM4 | National Oceanic and Atmospheric Administration, Geophysical Fluid Dynamics Laboratory, United States | 180 × 360, L33 | 0.31 | −0.58 | −1.47 |
| GFDL-ESM4 | — | 180 × 360, L49 | 0.33 | −0.38 | −0.91 |
| GISS-E2–1-G | Goddard Institute for Space Studies, United States | 90 × 144, L40 | 0.18 | −0.55 | −0.17 |
| GISS-E2–1-H | — | 90 × 144, L40 | 0.08 | −0.57 | −2.73 |
| HadGEM3-GC31-LL | Met Office Hadley Centre, United Kingdom | 144 × 192, L85 | 0.38 | −0.52 | −1.73 |
| UKESM1–0-LL | — | 144 × 192, L85 | 0.44 | −0.73 | −1.84 |
| INM-CM5.0 | Institute of Numerical Mathematics, Russia | 120 × 180, L21 | −0.02 | −0.16 | −0.01 |
| INM-CM4–8 | — | 120 × 180, L21 | −0.18 | −0.13 | 0.23 |
| IPSL-CM6A-LR | Institute Pierre Simon Laplace, France | 144 × 143, L79 | 0.56 | −0.23 | −0.30 |
| MIROC6 | Atmosphere and Ocean Research Institute (AORI), NIES, Japan Agency for Marine-Earth Science and Technology (JAMSTEC), Japan | 128 × 256 L81 | 0.51 | −1.28 | −2.37 |
| MIROC-ES2L | — | 64 × 128 L40 | −0.14 | −1.09 | −2.64 |
| MPI-ESM1–2-HR | Max Planck Institute for Meteorology, Germany | 192 × 384, L95 | 0.40 | −0.51 | −2.22 |
| MRI-ESM2–0 | Meteorological Research Institute (MRI), Japan | 160 × 320, L80 | −0.04 | −0.40 | −3.24 |
| NESM3 | Nanjing University of Information Science and Technology, China | 96 × 192, L47 | 0.34 | −0.38 | −0.65 |
| NorESM2-LM | NorESM Climate modeling Consortium consisting of CICERO, Norway | 96 × 144, L32 | 0.44 | −0.38 | −2.46 |

TABLE 2. Details of atmospheric model sensitivity experiments of CAM6/CESM2.

| Experiment | Description and method |
|---|---|
| CNTL | This is a 21-yr simulation, in which CAM6/CESM2 is forced by a climatological SST averaged from 1950 to 2015. The last 18 years are used in this study. The initial condition is AD 2000. |
| El Niño | Same method as CNTL, but model is forced by a composited El Niño SST. To generate the SST forcing, all El Niño events during 1950–2017 are composited according to the Niño-3.4 index. |
| CMS_neg | We extract the negative SSTA in the region of 120°E–180°, 5°–40°N from the composited El Niño SST. This negative SSTA is then added back to the climatological SST. |
| CMS_pos | Same method as CMS_neg run, but the treatment is only applied for the positive SSTA in region of 120°E–180°, 5°–40°N. |
| CMS_all | Same method as CMS_neg run, but both positive and negative SSTA in region of 120°E–180°, 5°–40°N are considered. |

$$\rho C_p h\frac{\partial T}{\partial t} = -\rho C_p h\mathbf{v}\cdot\nabla T - \rho C_p h w_e\frac{\partial T}{\partial z} - \rho C_p k_z\frac{\partial T}{\partial z} + \mathrm{SW} + \mathrm{LW} + \mathrm{LH} + \mathrm{SH}, \quad (3)$$

where $C_p = 4218\ \mathrm{J\ kg^{-1}\ K^{-1}}$ is specific heat of water, $h$ is the mixed layer depth (m), $\mathbf{v}$ is the horizontal flow, and $\rho$ is the density of seawater ($\mathrm{kg\ m^{-3}}$). The right-hand side of the equation is the combined forcing of the diffusive heat flux at the bottom of the mixed layer $T_{\mathrm{dif}} = -\rho C_p k_z(\partial T/\partial z)$, the vertical averaged advection term $T_{\mathrm{adv}} = -\rho C_p h\mathbf{v}\cdot\nabla T$, entrainment at the base of ocean mixed layer $T_{\mathrm{ent}} = -\rho C_p h w_e(\partial T/\partial z)$, surface longwave (LW) and shortwave (SW) heat fluxes, sensible (SH) and latent (LH) heat fluxes. In the downgradient diffusion model of $T_{\mathrm{diff}}$ term, $k_z$ is the Richardson number–based coefficient. In the budget analyses, the climatological annual cycles are removed, and we set $T_{zz} = T_{\mathrm{ent}} + T_{\mathrm{diff}}$.

### c. *Sensitivity experiment designs*

#### 1) ATMOSPHERIC GENERAL CIRCULATION MODEL EXPERIMENTS

To investigate the contributions of SSTA over EAMS in the maintenances of WNPac, we perform several SST pattern sensitivity experiments by using the Community Atmosphere Model, version 6 (CAM6), which is the atmospheric component of Community Earth System Model, version 2.11 (Danabasoglu et al. 2020). The sensitivity experiments contain one benchmark experiment and four sensitivity experiments, which are listed in Table 2. In the reference run, CAM6 is configured with 30 vertical levels and horizontal resolution of 1°. It is forced by the prescribed climatological SST averaged from 1950 to 2015. For the sensitivity experiments, we select and composite all El Niño events during the period from 1950 to 2015 based on the Niño-3.4 SST index. The composited global SST of El Niño is then applied to force CAM6, to understand the impacts of local and remote SST and sea ice in regulating WNPac. To highlight the contributions of positive SSTA over EAMS, we further extract the positive SSTA from the composited El Niño SST within the domain 120°E–180°, 5°–40°N and then retain it in the pattern of climatological SST while leave the SSTs outside this region at the climatological values (named CMS_pos). A similar treatment is also applied for the negative SSTA and dipole SSTAs within the domain 120°E–180°, 5°–40°N, which are named CMS_neg and CMS_all, respectively. All five experiments are run for 21 years; the outputs of the last 20 years are used in our analysis.

#### 2) PACEMAKER-COUPLED EXPERIMENTS

Second, to close the low cloud–SST feedback loop and learn its effects on the maintenance of SSTA and WNPac, this study conducts a series of pacemaker-coupled experiments using CESM2 with the altered low-level cloud fraction, cloud water content and feedback over EAMS, which are listed in Table 3.

The pacemaker-coupled experiment is a fully coupled simulation that contains all components as in the regular fully coupled simulations, but with SST restored to the model climatology plus observed historical anomaly in some high climate impact regions. In this study, the SST is restored in the equatorial east Pacific Ocean (15°S–15°N, 180°–280°E) while the air–sea interaction still operates freely over EAMS, to understand the behavior of low cloud over EAMS in the context of El Niño.

Following Global Monsoons Model Intercomparison Project Tier-2 (Zhou et al. 2016), the model diagnosed SST of CESM2 is restored to the corresponding constructed daily climatological SST, as follows:

$$\frac{\partial \mathrm{SST}}{\partial t} = \left.\frac{\partial \mathrm{SST}}{\partial t}\right|_{\mathrm{orig}} + \mathrm{coef}\frac{(\overline{\mathrm{SST}} + \mathrm{SST}') - \mathrm{SST}}{\mathrm{timescale}}, \quad (4)$$

where, $(\partial \mathrm{SST}/\partial t)|_{\mathrm{orig}}$ is the original SST tendency, $\overline{\mathrm{SST}}$ is the daily climatological SST, and SST′ is the anomaly. The restoring time scale is 10 days in this study. "Coef" represents the restoring coefficient, which is 1 in the equatorial east Pacific Ocean (15°S–15°N, 180°–280°E) and linearly reduced to 0 in a border buffer zone (20°S–20°N, 175°–285°E), as shown in Fig. A1 in appendix A.

This study applies two ways to construct the climatological-daily SST for restoring: one is the seasonally evolved daily mean SST during 1870–2015 based on the CESM's historical simulation, and the other is that simulated climatological daily SST plus the observed daily SSTA of all El Niño events in the period from 1870 to 2015. The former configuration reproduces the climate mean state of atmospheric circulation as a

TABLE 3. Details of pacemaker-coupled experiments of CESM2.

| Experiments | Restoring SST | Parameter of CLUBB |
|---|---|---|
| PACE_Climo | The SST in the equatorial east Pacific is restored to the daily climatology SST from a 145-yr CESM simulation (1870–2015). Atmospheric and oceanic components are freely coupled in the rest of areas. Please see Fig. A1 for the restoring area. | The whole globe has $C_8 = 4.2$, the coefficient of Newtonian pressure damping term of the third moment of vertical velocity. |
| PACE_Nino (a standard El Niño run) | Same as PACE_Climo, but the SST of equatorial east Pacific is restored to the observational anomalies of all El Niño Events during 1870–2015 plus the model climatology. | The whole globe has $C_8 = 4.2$. It offers an original low cloud–SST feedback over EAMS. |
| PACE_Nino_STRFB (a stronger positive cloud feedback only over EAMS in El Niño conditions) | The treatment of equatorial east Pacific SST is consistent with PACE_Nino run. | $C_8$ is 2 *only* over the EAMS domain (box in Fig. 1). For the rest of the areas, C8 = 4.2, which is consistent with above two experiments. |
| PACE_Nino_WKNFB (a weak cloud feedback over EAMS in El Niño conditions) | The treatment of equatorial east Pacific SST is consistent with PACE_Nino run. | $C_8$ is 6 over the EAMS domain (box in Fig. 1). |

reference (hereafter PACE_Climo). The latter is applied to reproduce the circulations of El Niño events, namely, the PACE_Nino run. The atmospheric response during El Niño winter and subsequent spring can be learned from the difference between these two types of experiments.

Now we perturb the low clouds in the EAMS domain (box in Fig. 1) based on PACE_Nino to learn the contributions of cloud feedback to the positive SSTA and WNPac maintenances during the El Niño winter and subsequent spring. To achieve this, we perturb the Newtonian pressure damping of the third-order vertical velocity $\overline{w'^3}$ of Cloud Layers Unified by Binormals (CLUBB), which represents turbulence, stratiform cloud macrophysics and shallow convection in CESM2 (Golaz et al. 2002; Larson 2017; Larson and Golaz 2005). The perturbations of Newtonian pressure damping explain most of the total variance of low cloud and shortwave cloud-radiative forcing (SWCF) over EAMS, due to the local warm SST and heating fluxes (Guo et al. 2015). A weaker Newtonian pressure damping provides less restriction of $\overline{w'^3}$, allowing stratocumulus to transform more quickly into cumulus clouds, thus reducing low clouds and SWCF, while the reverse is true for stronger damping (Guo et al. 2014; Larson 2017). Therefore, in the PACE_Nino_STRFB, we obtain stronger cloud feedback by reducing the coefficient of Newtonian pressure damping ($C_8$) from 4.2 to 2 in the EAMS (box in Fig. 1). Conversely, we conduct an opposite experiment with *weaker* cloud feedback in EAMS by enhancing the Newtonian pressure damping ($C_8 = 6$), namely, PACE_Nino_WKNFB. Since the only difference between PACE_Nino_STRFB, PACE_Nino_WKNFB, and PACE_Nino is the low cloud response in the EAMS domain, comparing the three gives an idea of the role of low cloud feedback (Table 3).

All four pacemaker-coupled experiments of CESM2 are configured with F09_G16 horizontal resolution (about 1° in both the atmospheric and the ocean components) and run for 11 years; the outputs of the last 10 years are used in our analysis. Please refer to appendix B for more details.

## 3. The low cloud–SST feedback during El Niño year

The climatological mean low cloud fractions and SST over the EAMS domain during winter and spring (DJFMAM) are shown in Fig. 1. The low cloud belt extends from southeastern China eastward to North Pacific (Figs. 1a and 2a). The low cloud, which is mainly composed of stratocumulus, stratus, and nimbostratus (by ISCCP's definitions), is the most frequent cloud type, exceeding 80% of the total cloud amount over the coastal area of southeastern China. SWCF dominates the net cloud-radiative forcing (NETCF). Correspondingly, SWCF and NETCF centers are located above southeastern China, EAMS, and the North Pacific (Figs. 1b,c), because of the dominance of low clouds. Notably, SWCF also shows a high center in the western Pacific, where there is a deep convective cloud regime. The deep cumulus is optically thick for both the SWCF and longwave cloud-radiative forcing (LWCF). Therefore, the western Pacific remains NETCF neutral in the normal years.

The El Niño–related SSTA and low cloud fraction anomalies are obtained through regressions against the December–February mean Niño-3.4 index. Both ICOADS and HadISST datasets show a positive SSTA extends from the East and South China Seas and the North Philippines Sea to the north of the WNP, while the WNP sees a negative SSTA during an El Niño year (Figs. 1h and 2d). Over the positive SSTA, there is a reduction in low cloud fraction in both ISCCP and ICOADS (Figs. 1e and 2c) and thereby a positive anomaly of SWCF (Fig. 1f), closing a strong positive low cloud–SST feedback loop between anomalous surface temperatures, anomalous cloudiness and SWCF over EAMS. Namely, the low cloud is to decrease as the local SST warms, which leads to a

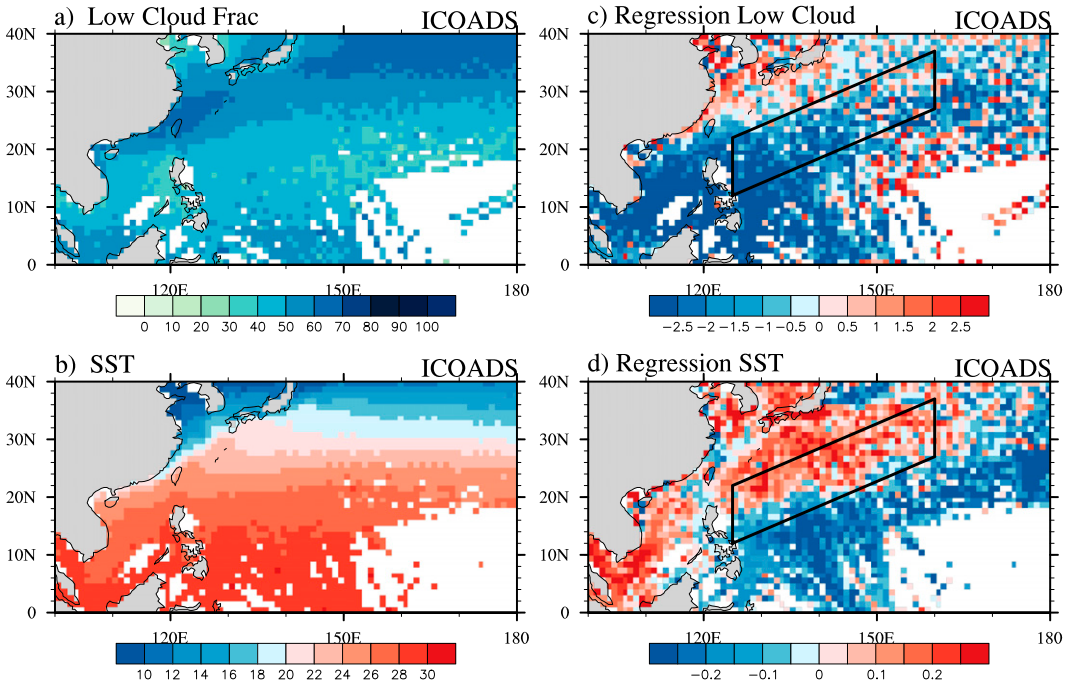


FIG. 2. (a) Climatological DJFMAM mean low cloud fraction (%) from ICOADS; (b) climatological DJFMAM SST (°C) from ICOADS. The (c) DJFMAM mean low cloud fractions and (d) SST from ICOADS regressed against the time series of DJF-mean Niño-3.4 index (%). ICOADS agrees well with ISCCP, that there is a strong negative correlation between low cloud fraction and SST.

shortwave warming that further enhances the initial warm SST.

The regressions of ISCCP marine low cloud fractions are in good agreement with ICOADS over the EAMS, indicating the reliability of our conclusions. The disagreement between ISCCP and ICOADS cloud-fraction anomalies over equatorial western Pacific is partly due to the different methods of categorizing cloud types in satellite retrievals and human observers (Clement et al. 2009) and the definition of low cloud in ISCCP. We also note that a large positive SWCF anomaly exists in the western Pacific (Fig. 1f), where there is a deep convective cloud regime. It is mainly related to convective suppression and thereby the reduction of total cloud fraction during El Niño (Cess et al. 2001). Due to the convective suppression, the low cloud fraction increases and thus has a positive correlation with the SSTA. However, this process is ignorable because low cloud is not highly weighted in the western Pacific. Moreover, the positive SWCF anomaly is compensated by a negative LWCF anomaly due to the decreased cloud-top altitude (Cess et al. 2001), which is the cloud altitude feedback (Hartmann and Larson 2002). It is evident in Fig. 1g, in which regional mean NETCF shows a weak negative anomaly in the western Pacific, but it is beyond the scope of this study.

To further understand the low cloud–SST feedback, we examine the interannual variations of SSTA and marine low cloudiness in the EAMS (Fig. 3a). The anomalies are calculated over the box shown in Fig. 1. The low cloud fraction is negatively correlated with the SSTA, in particular in El Niño winter and spring. A strong negative correlation between low cloud fraction and net surface shortwave flux is evident in ISCCP (not shown), which is due to the dominance of low clouds in DJFMAM. Notably that the relationships of cloud fraction and SSTA between 1976 and 1980 in Fig. 3a are not as robust as in other periods, as more than half of the ICOADS data are invalid in the EAMS during this period.

The monthly mean temporal tendencies of SST, LH, SH, and incoming LW and SW flux anomalies at the surface (averaged over EAMS) during El Niño years are shown in Fig. 3b. The Decembers of an El Niño year witness less low cloud fraction therefore more incoming shortwave flux at the surface. The SSTA exhibits an increasing tendency from December onward, when the latent heat flux dominates in the SSTA budgets. LW and the vertical averaged advection of the oceanic mixed layer play as the main sinks of the SSTA. The diffusion and entrainment of the oceanic mixed layer are usually small. The rest all show positive contributions to the SSTA budgets. After December, the latent flux decreases, while the positive net SW anomalies remain large until the subsequent April. During this period, the positive SSTA continues to increase. After February, the positive net SW anomalies start to overwhelm the latent heat flux in the SSTA budget. Moreover, the synchronous growth of the SSTA and shortwave radiation flux (and, by proxy, low cloud fraction) implies a positive low cloud–SST feedback, which is beneficial to the maintenance of local warmer SSTA after February. After May, following the onset of the summer monsoon, the prevailing cloud regime changes in this region, and the low cloud fraction and net SW

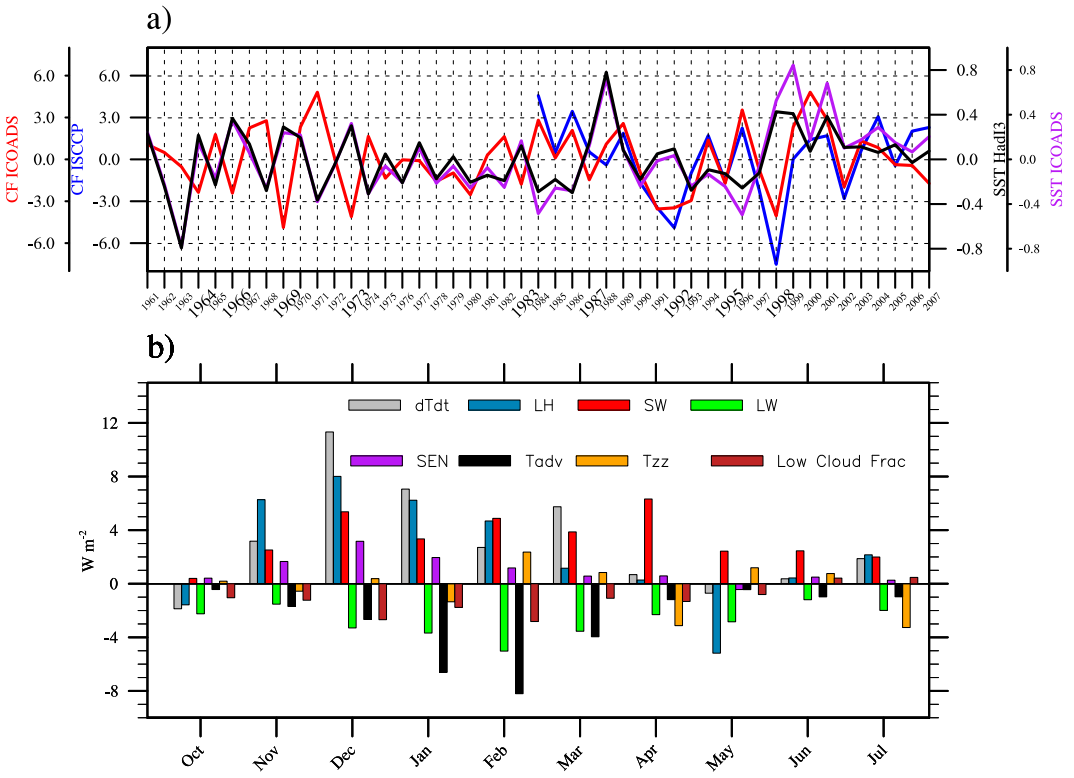


FIG. 3. (a) Interannual variations of the low cloud fraction from ISCCP (blue), low cloud fraction from ICOADS (red), and SST anomalies (black and purple) within the box shown in Fig. 1 during winter and spring (DJFMAM), the El Niño years are highlighted. (b) Budget analysis of the temperature equation (W $m^{-2}$) for the box shown in Fig. 1. Each term is regressed against the DJF-mean Niño-3.4 index. The anomalies of low cloud fraction are also shown in brown bars. Note, the climatological annual cycles and the longtime tendency are removed. There is a negative correlation between the low cloud fraction anomalies and SSTA over EAMS; the incoming solar radiation is one of the major source terms for the SST tendency.

flux anomalies decouple from the SSTAs, indicating that the low cloud–SST feedback no longer exists.

The above evidence demonstrates that the reduction of low cloud in the winters and subsequent springs of El Niño decaying years is crucial to the establishment of positive SSTA in the EAMS and therefore the corresponding low cloud–SST feedback.

Before we examine the circulation changes that dominate the low cloud changes, we recall that in the climate mean state the EAMS is covered by low-level clouds in DJFMAM (Figs. 1a and 2a). The low-level cloud is the most frequent cloud type, exceeding 80% of the total cloud amount over the coastal area of southeastern China (Fig. 1a). Two processes favor the formation of these low clouds:

First, the robust winter monsoon circulation suppresses the vertical penetration of convective clouds. Moreover, the relatively cold SST over the EAMS suppresses the vigorous turbulence for initializing deep convection. Both mechanisms promote a well-mixed and weakly entraining boundary layer that is favorable to low clouds (Fig. 4). In the *CALIPSO* dataset, therefore, the 2007–17 climatological mean cloud profiles are mainly located beneath 3–4 km over EAMS (Fig. C1 in appendix C). Notably, the *CALIPSO* dataset produces a higher cloud top than those derived from the passive remote sensors (like ISCCP) and reanalysis (e.g., ERA-Interim), because of its active remote sensors (Stubenrauch et al. 2013). This phenomenon is also present in eastern Asia (Li et al. 2017). Nevertheless, the predominance of low clouds and shallow boundary layers in the EAMS is also conclusive in *CALIPSO*.

Second, the divergence of subtropical westerly jet over the East Asian coastline is also beneficial to the formation of low stratiform clouds. The continental stratiform clouds in the leeside of the Tibetan Plateau are formed by shallow upward motions, which are caused by the surface-blocking effect in the absence of deep clouds of the Tibetan Plateau on the low-level westerlies (Yu et al. 2004). Due to the strong surface drag, a strong capping inversion and the mass divergence of the westerly flow at 500 hPa (Fig. 5a), the continental clouds extend downstream of the midlevel westerlies, adding to the prominent low cloud cover over the EAMS.

Low clouds reflect solar radiation and provide a net cloud-radiative cooling effect. Therefore, the low cloud belt is tightly coupled with the relatively cold SST over the EAMS. But, during El Niño winters and subsequent springs, the balance between the low cloud and SST cannot be maintained

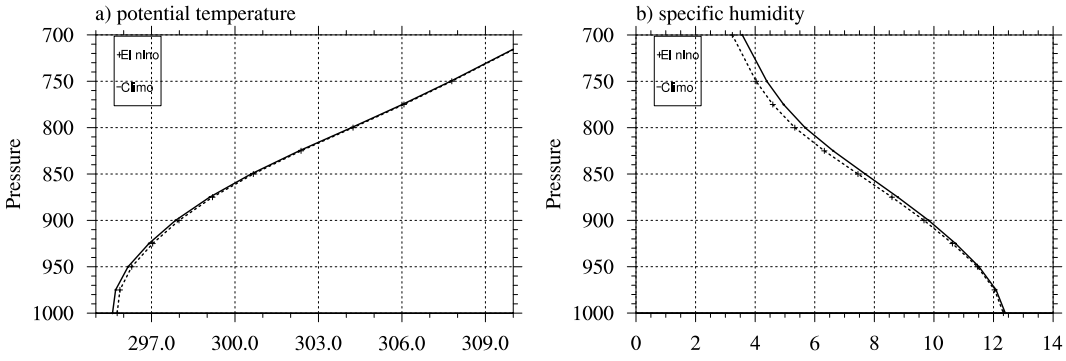


FIG. 4. Vertical profiles of (a) potential temperature (K) and (b) specific humidity (g $kg^{-1}$) averaged over the box area shown in Fig. 1 during winter and spring. Solid lines and dashed lines are the climatological means and anomalies in El Niño events, respectively. The EAMS stratification becomes weaker during El Niño years.

due to changes in the stability of the boundary layer and surface turbulence fluxes. These changes are explained in detail below:

The negative SSTA in the western Pacific warm pool suppresses convection there and leads to an anomalous anticyclone over the Philippines Sea at 850 hPa. On the northern side of the anticyclone, the anomalous southerly wind encounters the subtropical westerlies, leading to anomalous convergence (Figs. 5d,f). Also, the western flank of WNPac reduces the climatological southward moisture transport, leading to an accumulation of moisture and high moist enthalpy in the north of the anticyclone (Fig. 5f). They reduce the surface latent heat fluxes, lower-troposphere stability and low clouds, but enhance the local positive SSTA, upward motions, and precipitation (Fig. 6a).

There is an anomalous midtropospheric cyclone located over the northwestern side of the Philippines and southeastern China that causes anomalous convergence over southeastern China that weakens the divergence of climatological westerlies at 500 hPa (Figs. 5a,b). Therefore, in southeastern China and along the East China coast, the formation and the extension of continental low clouds are also weakened. Following this reduction of low cloud fraction, the net shortwave flux into the ocean surface increases (Fig. 6c).

The marine boundary layer becomes less stable, following the formation of positive SSTA. Due to the positive SSTA, both the inversion strength and the large-scale subsidence are weakened (Figs. 6a,d). It promotes a weakly stratified boundary layer with stronger vertical thermodynamic gradients (Fig. 4), which reduces the surface moisture supplied to low clouds and allows more entrainment of dry air at the top of the boundary layer (Fig. 6b). It favors the transition of stratocumulus to cumulus. In addition, the warmer sea surface emits more longwave radiation and tends to enhance the evaporation at the cloud base, which also leads to the break of low clouds.

In brief, these processes promote a positive low cloud–SST feedback over EAMS. The fraction of low cloud decreases in response to the positive SSTA and circulation changes. It increases the net shortwave flux into the ocean and helps to maintain or even enhance the local positive SSTA.

## 4. The low cloud–SST feedback helps to maintain the WNPac

In the previous section, we have shown how a collapse in the amount of low cloud over the EAMS can occur in response to El Niño–induced circulation changes. In this section, we investigate the effects of the positive low cloud–SST feedback and its underlying SSTA on the anomalous circulations themselves. We seek to understand how the amount of low cloud feedbacks on the strength of the WNPac. In particular, does the breakdown of low clouds in El Niño mature winters help to maintain the WNPac into the subsequent spring and early summer? Before answering this, we need to assess whether the cloud–SST feedback is present in coupled models. To do so, we analyze the historical experiments of 27 coupling models from CMIP6, as listed in Table 1. For each CMIP6 model, we pick out all El Niño events during 1850–2015 when its own standardized DJF-mean Niño-3.4 index exceeded one standard deviation. For those El Niño events, the correlation coefficients between the anomalous SWCF and SSTA are applied to quantify the strength of the low cloud–SST feedback over EAMS (box in Fig. 1). Generally, 20 out of 27 CMIP6 coupled models show similar positive correlation coefficients between SSTA and SWCF in El Niño events to observation, indicating the positive low cloud–SST feedback over the EAMS is also robust in climate models.

Out of the 27 CMIP6 models, 23 perform reasonably well in simulating the spatial patterns and circulation strengths of the WNPac as well as the observed positive SSTA over EAMS (not shown). We further define a vorticity index as the regionally averaged vorticity at 850 hPa over the domain 125°–150°E, 5°–30°N for quantifying the circulation strength of WNPac in the CMIP6 models. To understand the role of the low cloud–SST feedback in the maintenance of the WNPac, Fig. 7 examines the relationship between the strengths of WNPac and SWCF–SSTA correlation coefficients among CMIP6 models. Interestingly, the indexes of WNPac are highly consistent with the strengths of low cloud–SST feedback (Fig. 7). Namely, most models agree that the strength of positive low cloud–SST feedback and the index of WNPac have correlated increases. It implies the low cloud–SST feedback and its underlying positive

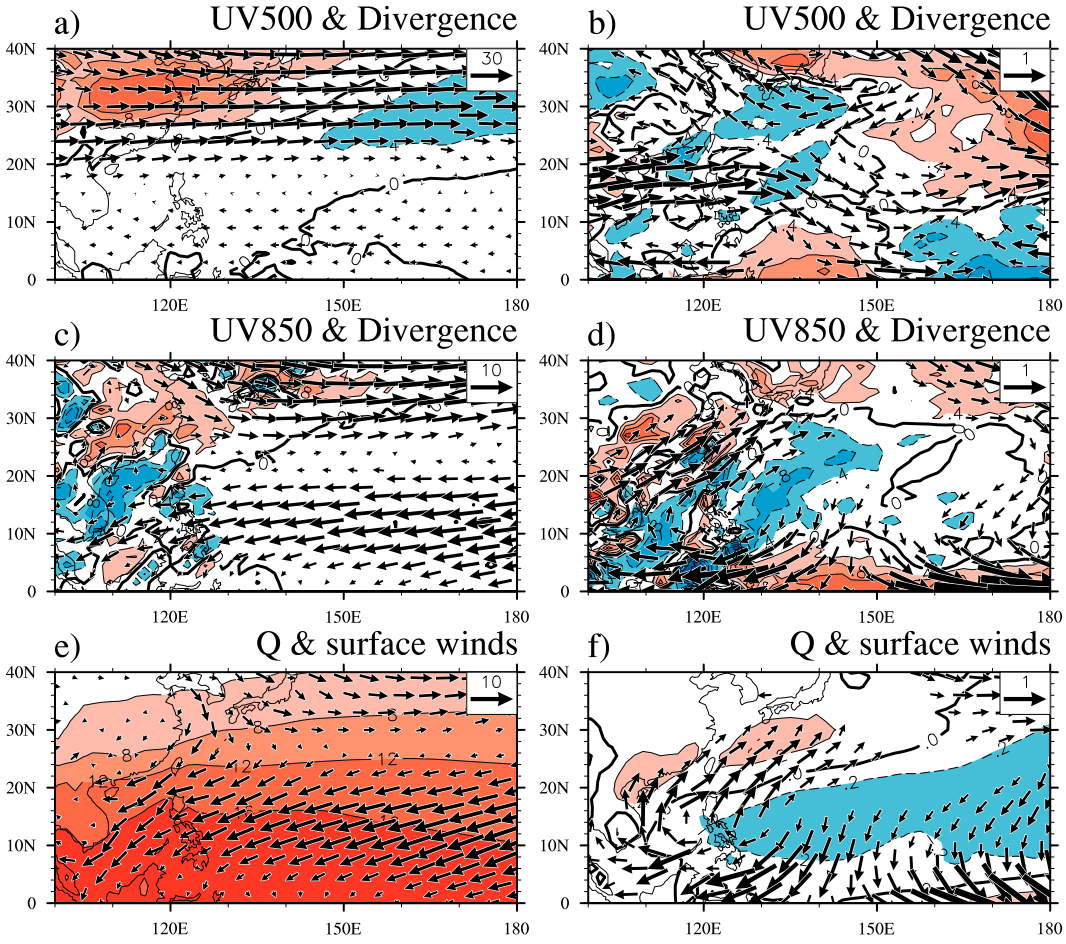


FIG. 5. (a) DJFMAM mean 500-hPa climatological winds (vectors; m $s^{-1}$) and divergence (shading; $10^{-6}$ $s^{-1}$) and (b) anomalous winds and divergence at 500 hPa regressed against the Niño-3.4 index; (c),(d) as in (a) and (b), but for 850 hPa; (e),(f) as in (a) and (b), but for the moisture transports (g $kg^{-1}$ m $s^{-1}$) and specific humidity (g $kg^{-1}$) at 1000 hPa. The large-scale circulation responses are beneficial to the reduction of low clouds.

SSTAs over the EAMS is a possible mechanism for maintaining the WNPac.

It is also notable that the scatters positions of five coupled models, such as FGOALS-f3-L, MIROC6, MIROC-ES2L, CESM2, and IPSL-CM6A-LR, are a bit far from the regression line and the rest of scatters. As WNPac is maintained by both the local air–sea interactions over the west northern Pacific and the remote forcing from the equatorial central-eastern Pacific (Wu et al. 2017a). The contributions of the two maintenance mechanisms highly depend on the dynamical cores and physics schemes of models. If one of the maintenance mechanisms is stronger in a model, it would somewhat overshadow the contributions of the other one. For example, the negative precipitation anomalies over the tropical WNP (2°–15°N, 125°–160°E) are −2.38 mm $day^{-1}$ in FGOALS-f3-l, −2.37 mm $day^{-1}$ in MIROC6, −2.64 mm $day^{-1}$ in MIROC-ES2l, and −2.6 mm $day^{-1}$ in CESM2, which are much larger than the multiple model ensemble mean (−1.37 mm $day^{-1}$). The stronger negative precipitation anomalies over the tropical WNP favor stronger Rossby wave–like responses at the lower troposphere, as well as a stronger WNPac. One can infer from this that these four climate models would represent stronger WNPacs than the multiple model ensemble mean does, even if the low cloud feedbacks of these models may not be very strong. However, these four models still show concurrent increases in the strengths of low cloud–SST feedback and WNPac circulation (Fig. 7). For example, among these four climate models, MIROC-ES2l has the weakest low cloud feedback and also has the weakest WNPac. Conversely, if the contribution of low cloud feedback is strong, the contribution of precipitation could be less important. IPSL-CM6A-LR has the weakest negative precipitation anomalies (only −0.3 mm $day^{-1}$) over the tropical WNP of the coupled models that successfully reproduce the WNPac, but its circulation strength of WNPac is still greater than almost 40% of the CMIP6 climate model, due to its strong low cloud feedback.

One may argue that the robust positive linear relationship of low cloud–SST and WNPac among the CMIP6 models may only indicate that the positive SSTA and low cloud feedback over EAMS are the consequences of WNPac and do not fully

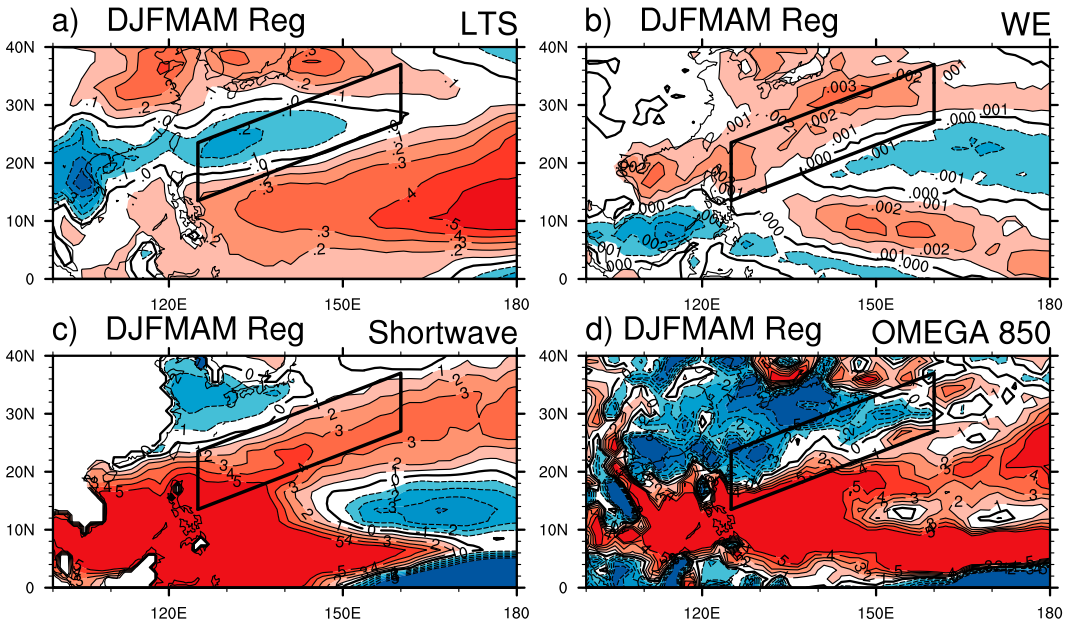


FIG. 6. The anomalies of (a) LTS (K), (b) entrainment rates (cm $s^{-1}$), (c) surface net shortwave flux (W $m^{-2}$; downward is positive), and (d) omega at 850 hPa (hPa $day^{-1}$) regressed against the Niño-3.4 index.

account for the role of low clouds in maintaining WNPac. However, we think the positive SSTA and low cloud feedback help to maintain the anticyclone by enhancing the positive/negative SSTA gradients in EAMS/WNP, the moist enthalpy advection and precipitation anomalies in WNP. To support this hypothesis, we performed a two-step numerical test: in the first step, we verify the importance of positive SSTA in the maintenance of WNPac through a series of SST sensitivity experiments based on CESM2's atmospheric component (Table 2). In this step, we are not claiming that there is a feedback between SSTA and WNPac; hence we may use fixed SSTs and prescribe the SSTAs. In the second step, we demonstrate the importance of local low cloud feedbacks in the maintenance of positive SSTA over EAMS and WNPac, by configuring a series of pacemaker-coupled experiments of CESM2 (Table 3). In this step, we do claim that there is a feedback between clouds and SST, and hence we perform coupled ocean–atmosphere simulations here.

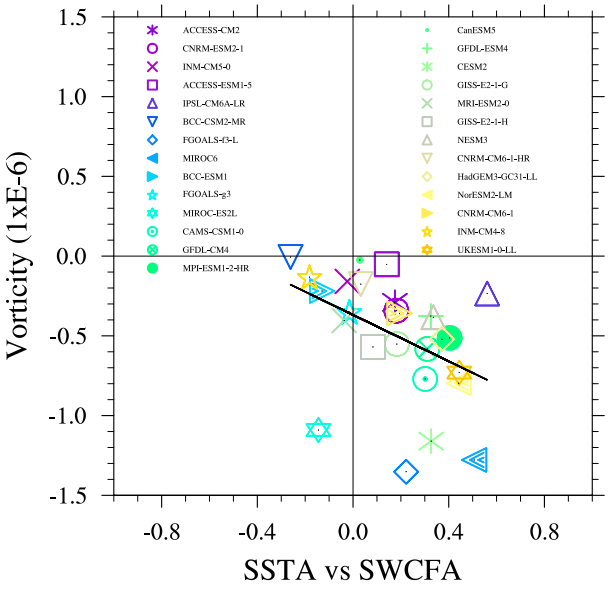


FIG. 7. CMIP6 models scatterplots of the DJFMAM vorticity indexes and the correlation coefficients between regional averaged SWCF and SSTA over EAMS during El Niño events. CMIP6 models agree that the low cloud feedback and WNPac's circulation strength concurrent increases.

Some points can be made from the series of prescribed SST sensitivity experiments. First, the local effects of positive/negative SSTAs over EAMS/WNP (120°E–180°, 5°–40°N) are not ignorable and do have significant contributions in regulating the WNPac. When CAM6/CESM2 is solely forced by the positive SSTA over EAMS, that is, the CMS_pos run shown in Fig. 8a, a positive anomalous precipitation and an anomalous cyclone are generated locally in response to the positive SSTA. Such positive anomalous precipitation is also evident in the observations (Wang et al. 2017). The southern branch of the anomalous cyclone would advect high-latitude dry air into the WNP and suppresses the local convection that helps to form an anomalous anticyclone over WNP at the southeast of the positive SSTA (Fig. 8a). But the location of this anomalous anticyclone is farther east than the reanalysis. Its area-averaged (130°E–180°, 5°–30°N) vorticity is $-0.8 \times 10^{-7}$ $s^{-1}$, compared to the WNPac vorticity index of $-4.3 \times 10^{-7}$ $s^{-1}$ in the multimodel ensemble mean of fully coupled CMIP6 models, and $-8.5 \times 10^{-7}$ $s^{-1}$ in reanalysis. Similarly, if only

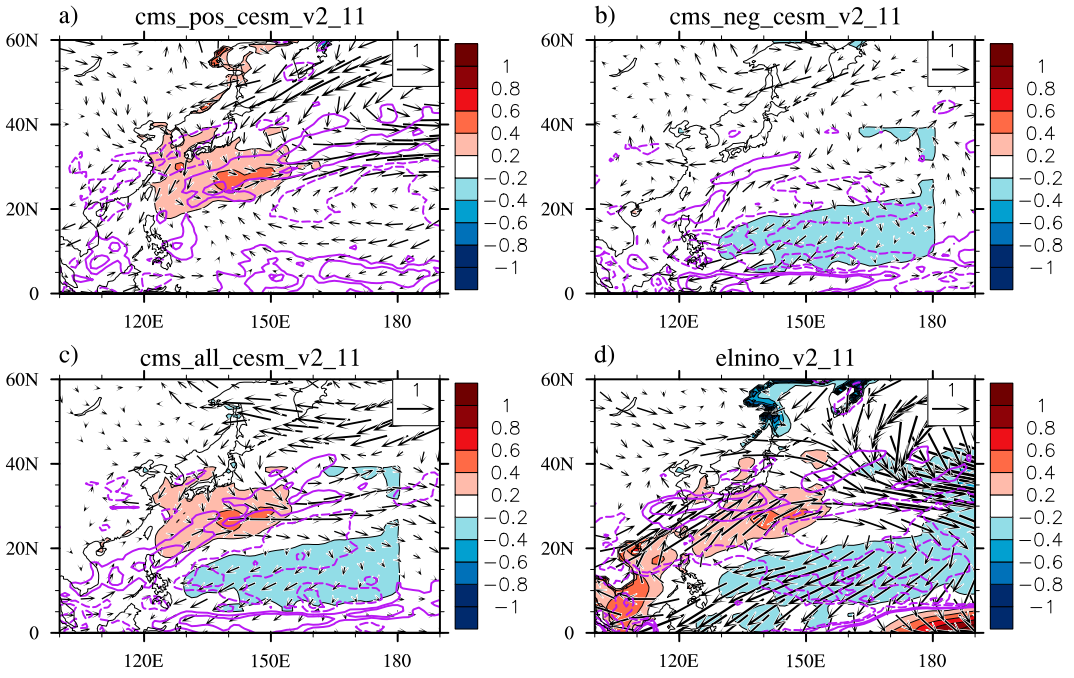


FIG. 8. The horizontal distributions of SST (shading; K; the prognostic sea ice surface temperature is also shown), anomalous precipitation (the solid and dashed purple contours denote positive and negative values, respectively; the contour interval is 0.3 mm day$^{-1}$) and 850-hPa winds (vectors; m s$^{-1}$) from (a) the difference between CMS_neg and CNTL run, (b) the difference between CMS_pos run and CNTL run, (c) the difference between CMS_all run and CNTL run, and (d) the difference between El Niño run and CNTL run.

the negative SSTA over the tropical western Pacific is imposed (configuration, CMS_neg run in Fig. 8b), an anomalous anticyclone over WNP forms with area-averaged vorticity index of $-3.3 \times 10^{-7}$ s$^{-1}$ in response to the negative SSTA and the suppressed convection. The results of CMS_neg agree with the mechanism of "wind–evaporation–SST" feedback suggested by (Wang et al. 2003). Although the negative SSTA produces a strong anticyclone anomaly, the positive SSTA contribution is also not ignorable, because it also provides negative vorticities to the anticyclone anomaly. Individually, the anomalous anticyclones in the CMS_neg and CMS_pos experiments are meridionally narrower and weaker than those in the reanalyzed data. The size of anomalous anticyclones becomes larger in zonal with its northwestern flanks enhanced, when the dipole SSTA pattern is applied in CAM6/CESM2 (Fig. 8c). In this case, the vorticity of WNPac increases to $-3.6 \times 10^{-7}$ s$^{-1}$.

Second, remote SSTA forcing can also impact the simulation of WNPac. In the benchmark experiment, namely, the El Niño run (Table 2), the global SSTA is applied as the forcing, as shown in Fig. 8d. The WNPac is well established in DJFMAM, which agrees with observations. In addition, the vorticity index of anticyclone further increases to $-6.9 \times 10^{-7}$ s$^{-1}$. It indicates that the tropical SST anomalies are responsible for the formation of the WNPac. The better simulation of anomalous anticyclone confirms the contributions of remote SSTAs, especially for the positive SSTA over the equatorial central-eastern Pacific.

By comparing these four atmospheric experiments, we can also observe that 1) our results are consistent with previous studies that show that the WNPac is formed through a Rossby wave–like response to the deficient rainfall over the tropical Pacific (Wu et al. 2017a,b); 2) our results are consistent with the conclusions of Wang et al. (2000) that a dipole pattern of warm/negative SSTAs over the WNP acts to maintain the WNPac. This positive SSTA can be considered as due in part to a breakdown of low cloud fraction in response to circulation changes in El Niño years, which, in turn, feeds back positively onto SSTs to strengthen these circulation changes.

The atmospheric experiments have well revealed the importance of EAMS positive SSTA in maintaining WNPac. To better reveal the effect of low cloud–SST feedback, we need to close the cloud feedback loop to investigate how the cloud influences the positive SSTA and thereby the intensity of WNPac. Hence, we conduct a series of pacemaker-coupled experiments using a fully coupled model CESM2 (Table 3), in which we also alter the magnitudes of low cloud–SST feedback over EAMS (the box in Fig. 1).

The PACE_Climo represents the climate mean state (Fig. 9a), in which the SST in the equatorial east Pacific Ocean (box area in Fig. A1) is restored to the daily climatology SST with the seasonal cycle from a 145-yr CESM historical simulation, while in the other areas the oceanic and atmospheric components of CESM2 are freely coupled. The winds at 850 and 925 hPa and low cloud fraction and SST in DJFMAM are shown in Figs. 9a and 10a. In the WNP, the simulated

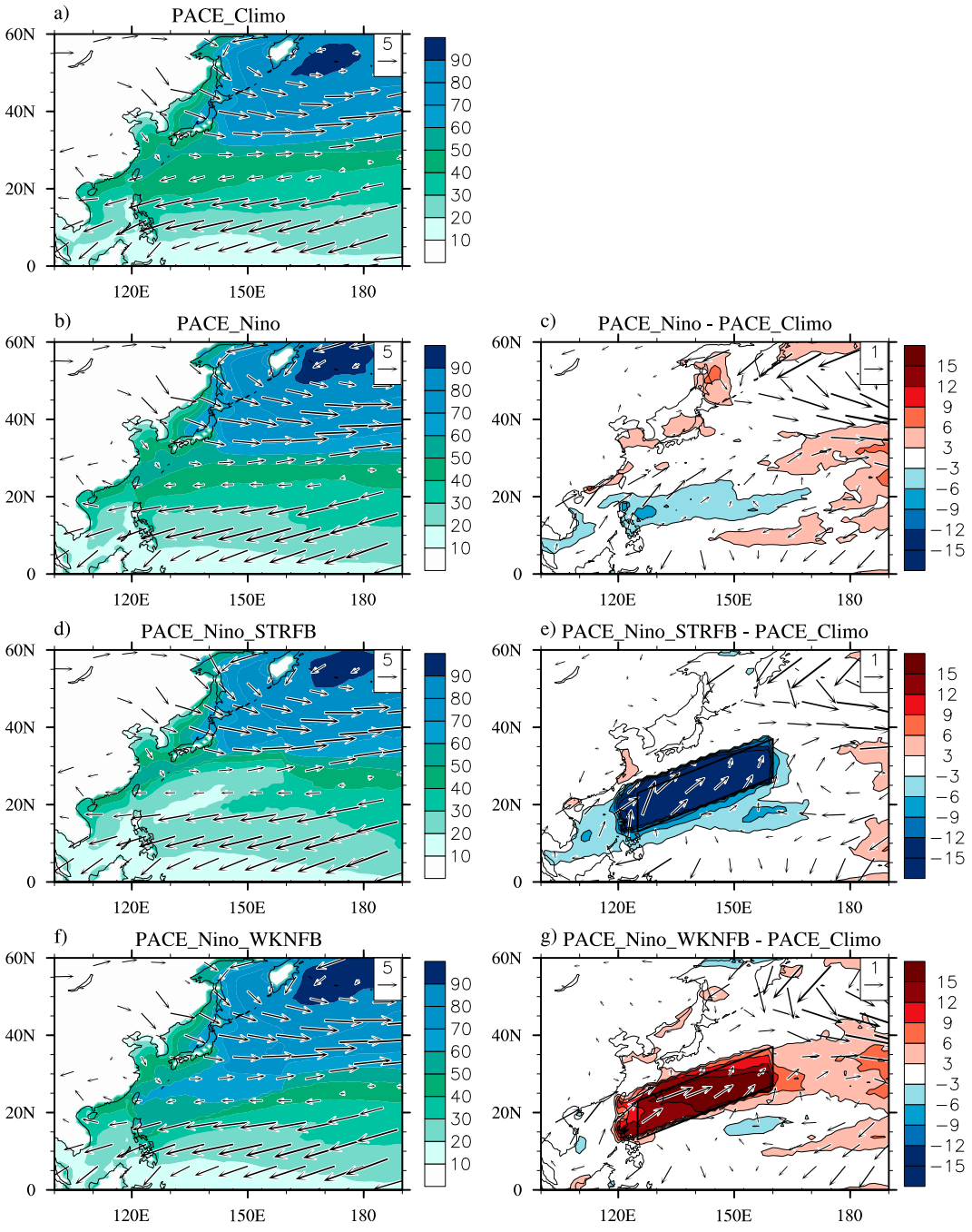


FIG. 9. Climatological mean low cloud fraction (shading; %) and 925-hPa winds (vectors; m $s^{-1}$) from (a) PACE_Climo, (b) PACE_Nino, (d) PACE_Nino_STRFB, and (f) PACE_Nino_WKNFB. (c),(e),(g) The differences between three El Niño runs in (b), (d), and (f) and PACE_Climo, respectively. The boxes mark EAMS domain where the Newtonian pressure damping is weakened or enhanced.

low cloud fraction and winds agree well with observations shown in Figs. 1 and 5.

The PACE_Nino run reproduces the atmospheric circulations during the El Niño events, since the SST in the equatorial east Pacific Ocean is restored to the sum of the simulated daily climatological SST and the observed daily SSTA of the El Niño event (Figs. 9b,c). The resultant anomalous circulations and low cloud fractions are obtained from the subtractions of the PACE_Nino run from the PACE_climo run, which are shown in Figs. 9c and 10c. Based on Fig. 9c, the low cloud fraction has a deficit of 5.1% over EAMS during the El Niño winter and subsequent spring. Such a low-level cloud

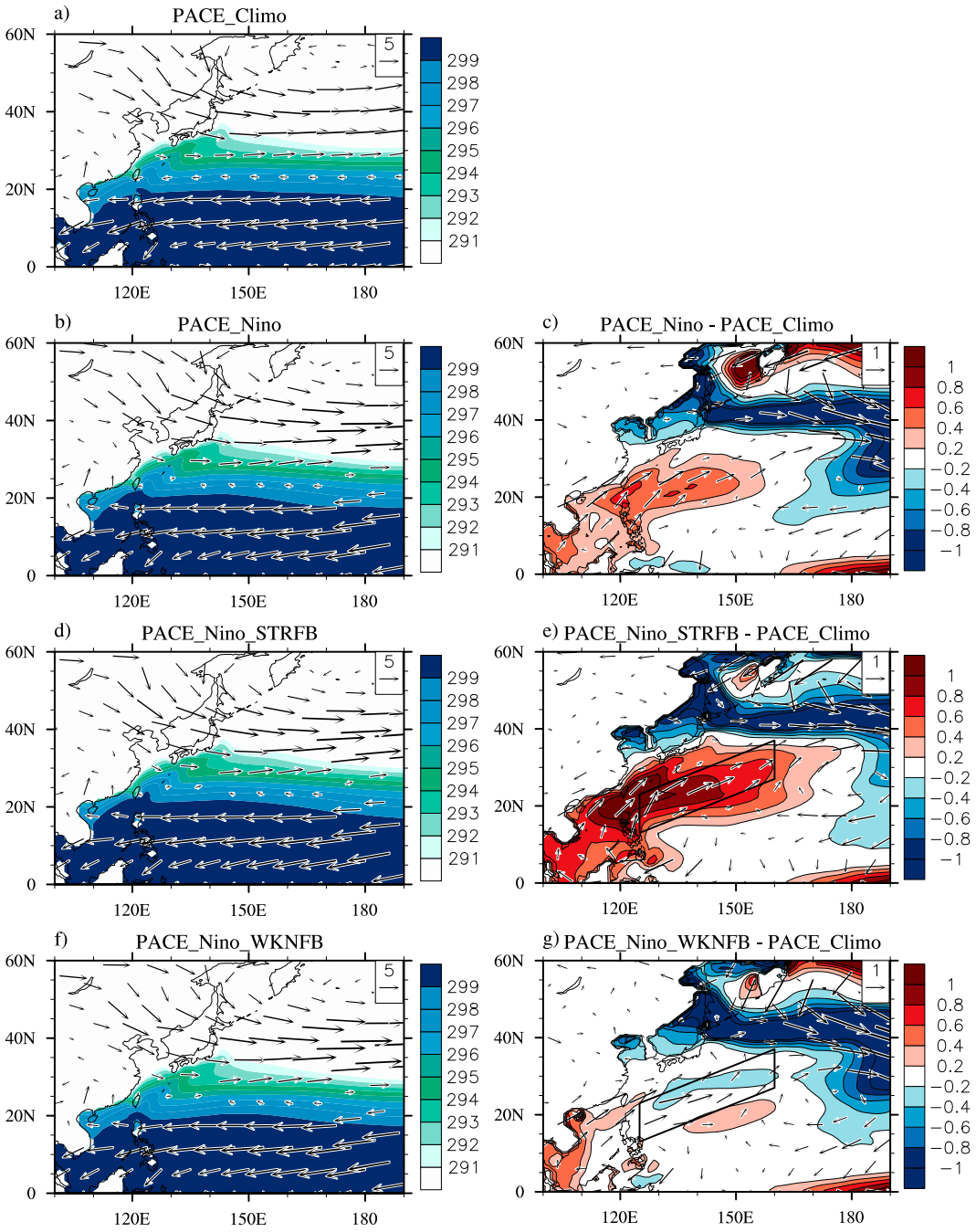


FIG. 10. As in Fig. 9, but for the SST (K; shading) and 850 hPa winds (vectors; m $s^{-1}$). If the SST over equatorial east Pacific is restoring to the observational anomalies of all El Niño events during 1870–2015 plus the model climatology, both WNPac and the positive low cloud feedback are well reproduced by the coupled model CESM2; if we build on this by further enhancing the strength of the low cloud feedback over EAMS (boxes), the circulation strength of WNPac enhances, and vice versa.

deficit reduces the cloud reflection and further weakens the cooling effect of SWCF by about 9.4 W $m^{-2}$ (not shown), which is helpful for the maintenance of the local positive SSTA (0.48 K) in EAMS (Fig. 10c). These results suggested that the observed positive low cloud–SST feedback over EAMS is also evident in pacemaker-coupled experiments. Correspondingly, WNPac generates with its vorticity index at 850 hPa of $-4.5 \times 10^{-7}$ $s^{-1}$, indicating the WNPac has largely resulted by both the remote forcing of SSTA over the east Pacific and the local cloud feedback, which is consistent with previous studies (Wu et al. 2017a,b).

The PACE_Nino_STRFB experiment is the same as the PACE_Nino in restoring SST, but we amplify the low cloud deficit and the cloud feedback only in the domain of EAMS (box in Fig. 9) by weakening the Newtonian pressure damping of third-order vertical velocity $\overline{w'^3}$ in CLUBB. This amplifies the cloud feedback because the Newtonian pressure damping of $\overline{w'^3}$ is one of the most influential processes for the low clouds and SWCF over EAMS (Guo et al. 2015), and the weaker pressure damping means the stratocumulus can more easily transit to the shallow convection (Golaz et al. 2007; Guo et al. 2014; Zhang et al. 2018).

As we mentioned earlier, the restoring SST is applied only in equatorial east Pacific and hence the EAMS cloud–SST feedback still operates freely in the PACE_Nino and PACE_Nino_STRFB runs. Thus, through the comparisons of the differences between PACE_Nino_STRFB, PACE_Nino and PACE_climo (Figs. 10c,e), the contributions of EAMS cloud–SST feedback to the maintenance of the WNPac are deduced while the atmospheric circulation anomalies of El Niño events are still retained to the greatest extent possible in both in PACE_Nino and PACE_Nino_STRFB. Due to the weaker Newtonian pressure damping in the turbulent scheme, the PACE_Nino_STRFB run dramatically expands the low cloud deficit even further from the PACE_Nino run (Fig. 9e), which leads to a further increase in the positive SSTA over EAMS (Fig. 10e). Specifically, the low cloud deficit grows to 16.4% and the positive SSTA becomes 0.84 K over EAMS, as we expected. If the low cloud–SST is quantified as the ratio between the regional averaged SWCF and SSTA, the feedback is 27 W $m^{-2}$ $K^{-1}$ over EAMS in PACE_Nino_STRFB, which is much larger than it in the PACE_Nino run (19.6 W $m^{-2}$ $K^{-1}$). The positive SSTA reduces the lower-troposphere stability but enhances the turbulent transports of moisture and heat. Consequently, the intensity of the WNPac in the PACE_Nino_STRFB run is $-7 \times 10^{-7}$ $s^{-1}$, which is also stronger than that in the PACE_Nino. The stronger WNPac and its northwestern flank in turn cause a further decrease in lower-troposphere stability with increased moisture in EAMS, as well as the low cloud deficit.

Now we ask the following: What happens if the low cloud anomaly becomes positive in the context of El Niño, say, the cloud feedback changes to negative from positive over EAMS? Based on the PACE_Nino run, we enhance the Newtonian pressure damping of $\overline{w'^3}$ in the PACE_Nino_WKNFB run, which means that the transition from stratocumulus to shallow convection slows down. As the SST grows over EAMS, the moisture turbulent mixing driven by local warm SST overwhelms the convective drying, generating more low clouds (Figs. 9f,g) and negative cloud feedback. Meanwhile, the restored El Niño SST in equatorial east Pacific has been warm enough on its own to form the WNPac. Once WNPac is generated, the anomalous southwesterlies on its western flank further weaken the climatological northeasterly trade winds and latent heat fluxes that act to generate the positive SSTA over EAMS. However, the shortwave cooling effect caused by the increased low cloud (−8.9 W $m^{-2}$) compensates for the warming effect of latent heat fluxes (5 W $m^{-2}$) and the cloud longwave heating to the surface (3.8 W $m^{-2}$), which finally prevents the formation of the positive SSTA in PACE_Nino_WKNFB. The SSTA is almost zero in EAMS and the vorticity index of WNPac weakens to $-2.3 \times 10^{-7}$ $s^{-1}$ in PACE_Nino_WKNFB (Figs. 10f,g).

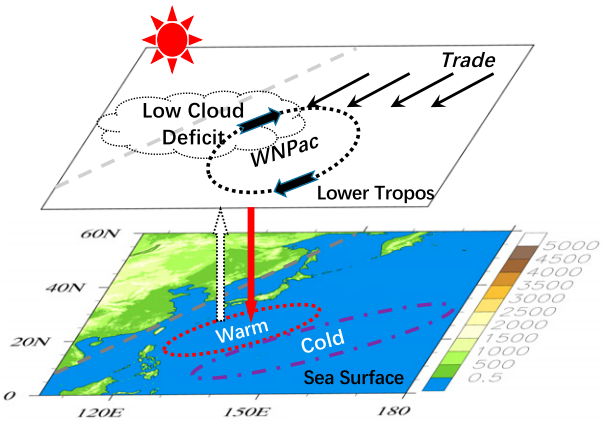


FIG. 11. Schematic diagram illustrating how the positive low cloud–SST feedback establishes and works over EAMS during the El Niño decaying winter and spring. In response to the suppressed convection over the warm pool, a WNPac (dashed curve and solid black arrowheads at lower troposphere) is established. Its western branch induces anomalous convergence resulting from blocked trades and moisture transport (thin black arrowheads). The deficit of low cloud further leads to enhanced shortwave fluxes (thick red downward arrowhead) and then a positive SSTA (dashed curve on surface). The SSTA further reduces the low clouds by destroying the boundary layer condition (dashed white upward arrowhead). The low cloud feedback and positive SSTA help to maintain the anticyclone through enhancing the positive/negative SSTA gradients in EAMS/WNP.

The concurrent weakening of the intensity of cloud feedback and WNPac from PACE_Nino_STRFB and PACE_Nino to PACE_Nino_WKNFB indicates that the positive low cloud–SST feedback does contribute to the maintenance of the WNPac.

## 5. Conclusions and discussion

In this study, we show that during DJFMAM of El Niño years, a positive low cloud–SST feedback operates in EAMS that the negative low cloud fraction anomaly, positive SWCF anomaly, and positive SSTA form the complete feedback loop. The physical mechanism of this feedback may be characterized by the following statements and the schematic diagram (Fig. 11):

In the DJFMAM climatology, the low cloud fraction belt that dominates total cloudiness and leads to cooling effects is tightly coupled with the cold SST over EAMS. First, the large-scale subsidence of robust winter monsoon circulation and strong lower-troposphere stability promote the formation of low clouds. Second, due to the drag effect and divergence of westerlies, the continental low cloud further extends to the downstream of westerlies. However, such a climatological balance is changed by atmospheric responses during El Niño winter and subsequent spring. The cooler SSTA in the western Pacific warm pool leads to an anomalous anticyclone over

the Philippines Sea. Its western branch reduces the surface moisture transports and latent fluxes in EAMS from ocean; it also causes anomalous convergence and weaker turbulent mixing in the atmospheric boundary layer, which reduces the low clouds. At 500 hPa, an anomalous cyclone over southeastern China inhibits the formation of continental low cloud by reducing the divergence of the midlevel westerlies. This further reduces low cloud fraction over the EAMS because less low cloud is advected over the adjacent oceans. The deficit of low clouds further leads to more incoming shortwave radiation and a positive SSTA over the EAMS. Once the positive SSTA appears, surface heating and buoyancy flux are enhanced while stratification weakens, producing a stronger entrainment rate and a weaker stratified marine boundary layer. Therefore, the low clouds, incoming solar radiation, and SSTA constitute a positive low cloud–SST feedback loop. Such positive low cloud–SST feedback plays an essential role in maintaining the positive SSTA in the EAMS, especially after February.

Based on the climate models, this study further reveals that this positive low cloud–SST feedback in EAMS plays as a possible maintenance mechanism for WNPac by enhancing the positive/negative SSTA gradients in EAMS/WNP. The positive low cloud–SST feedback is present in most of the fully coupled models from CMIP6, which simulate positive correlation coefficients between SSTA and SWCF. Moreover, CMIP6 coupled models show that the strengths of WNPac are highly consistent with the strengths of low cloud–SST feedback, that is, both of them have concurrent increases. SST perturbation experiments with CAM6 demonstrate that the positive SSTA in EAMS induces a positive precipitation anomaly and anomalous cyclone over EAMS, advecting high-latitude dry air into the WNP and reinforcing the anomalous anticyclone over WNP just south of the positive SSTA. To further elucidate the cloud feedback and its contributions, we conducted four idealized pacemaker-coupled experiments of CESM2, with the SST in the equatorial east Pacific Ocean restored to the model daily climatology and observational anomalies of El Niño events, respectively. If we restore only the positive observational SST anomalies over the equatorial east Pacific Ocean, CESM2 well reproduces the deficits of low clouds and the positive low cloud–SST feedback over EAMS. If we further enlarge the low cloud deficit and then the intensity of the cloud feedback on top of this, the circulation intensity of WNPac will increase because of larger SSTA gradients in EAMS/WNP. This indicates that the positive low cloud–SST feedback contributes to the maintenance of the WNPac.

As a caveat, we note that this study cannot precisely quantify the relative contribution of the cloud feedback to the intensity of WNPac, although we reveal that it facilitates the maintenance of WNPac by conducting pacemaker-coupled experiments with unrealistically strong/weak cloud feedbacks in EAMS. On one hand, the low cloud feedback continues to govern the model's uncertainty, which can be traced back to the different processes with separate physical assumptions in the model. The changes in these physical assumptions do have dramatic impacts on the intensity of feedback, just as previous studies have shown (Geoffroy et al. 2017; Medeiros et al. 2015; Neggers 2015). However, identifying and quantifying these individual processes' contributions to cloud feedback is difficult because the observation merely provides little details of the present day and is most likely the result of the competing effects of these unresolved processes (Ceppi et al. 2017; Klein and Hartmann 1993), and the large-eddy simulation still highly depends on the choice of microphysics schemes and SST (Bretherton et al. 2013; Tan et al. 2016). On the other hand, the simulation of WNPac is also influenced by other mutual processes and feedbacks, such as the precipitation over WNP and Indian Ocean, remote forcings, "wind–evaporation–SST," and "wind-induced moisture enthalpy," etc. Their relative importance also depends on the model-specific dynamical cores and physics schemes. However, despite the above uncertainties, we believe this study implies that low cloud–SST feedback in EAMS could provide an observational constraint on the simulations and projections of WNPac and East Asian monsoon.

*Acknowledgments.* This work is supported by National Key Research and Development Program of China (2020YFA0608903) and National Natural Science Foundation of China (42175164 and 41775102). Kalli Furtado has been supported by the U.K.–China Research and Innovation Partnership Fund through the Met Office Climate Science for Service Partnership (CSSP) China as part of the Newton Fund. This work is also supported by the National Key Scientific and Technological Infrastructure project "Earth System Science Numerical Simulator Facility" (EarthLab). The authors gratefully acknowledge helpful comments by Dr. Bo Wu, and three anonymous reviewers.

*Data availability statement.* The following datasets were downloaded from the following web pages: GODAS (https://www.cpc.ncep.noaa.gov/products/GODAS/background.shtml), ISCCP's D2 product (https://isccp.giss.nasa.gov), ERA-Interim (http://rda.ucar.edu), ICOADS (https://icoads.noaa.gov), and *CALIPSO* product (http://climserv.ipsl.polytechnique.fr/cfmip-obs/Calipso_goccp.html). Source code of CESM2, version 2.1.1, was downloaded from (https://www.cesm.ucar.edu/models/cesm2/?ref=hpb) and CMIP6 results was downloaded from (https://esgf-node.llnl.gov/search/cmip6/).

## APPENDIX A

### Restoring Regions and Coefficients for Pacemaker Experiments

Figure A1 shows the restoring regions and coefficients for pacemaker experiments. The restoring coefficient is 1 in the equatorial east Pacific Ocean (15S°–15°N, 180°–280°E) and linearly reduced to 0 in a border buffer zone (20°S–20°N, 175°–285°E).

## APPENDIX B

### Basis of Changing the Low Cloud Response and Feedback over EAMS

One of the difficulties of the experiments is how to enhance the low cloud–SST feedback in EAMS without changing the

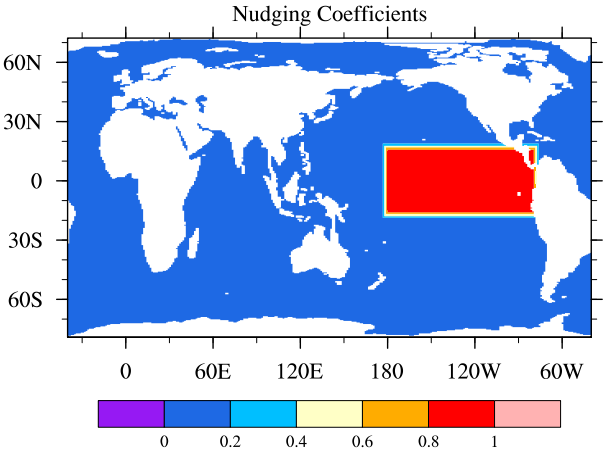


FIG. A1. The restoring regions and coefficients for pacemaker experiments.

responses of the atmospheric circulations in other regions to the El Niño SSTA. In this study, we perturb one single sensitive parameter (process) in the turbulence scheme of CESM2.

CLUBB is the default boundary layer scheme in CESM2. It offers a unified treatment for representing turbulence, shallow convection and cloud macrophysics (Golaz et al. 2002; Larson and Golaz 2005; Larson et al. 2002). As a unified scheme of cloud dynamics, CLUBB can partly reduce the uncertainties in cloud feedback introduced by the separate assumptions for subgrid variability of distinct physics schemes (Ceppi et al. 2017; Larson et al. 2012; Zhang et al. 2013).

Previous studies (Guo et al. 2015) have shown that the low cloud fraction, cloud water content and SWCF over EAMS are very sensitive to the perturbation of parameter $C_8$, namely, the Newtonian pressure damping of third-order vertical velocity $\overline{w'^3}$ in CLUBB, because of the relative large $\overline{w'^3}$ driven by the local warm SST and strong surface heating fluxes over EAMS. Our strategy is thus to change the low cloud feedback by perturbing $C_8$ (and then $\overline{w'^3}$) over the domain of EAMS (Fig. 1e). It can be demonstrated by a simplified $\overline{w'^3}$ prognostic equitation [Eq. (4.12) in Larson 2017]:

$$\frac{\partial \overline{w'^3}}{\partial t} \propto -\frac{1}{\rho_s}\frac{\partial \overline{w'^4}}{\partial z} + \frac{3g}{\theta_{vs}}\overline{w'^2\theta'_v} - \frac{C_8}{\tau}\overline{w'^3}\,C_{11}\left(3\overline{w'^3}\,\frac{\partial \overline{w}}{\partial z}\,\overline{w^2\theta'_v}\right), \tag{B1}$$

where a prime indicates the subgrid distributions, an overbar means averaged quantities of the grid scale, $\rho_s$ is the air density, $z$ is the height, $\theta_v$ is the virtual potential temperature, and $g = 9.8\ \mathrm{m\ s^{-2}}$ is the gravity constant.

Physically, the Newtonian pressure term $-(C_8/\tau)\overline{w'^3}$ and the buoyancy damping $-C_{11}[3\overline{w'^3}(\partial\overline{w}/\partial z) + (3g/\theta_{vs})\overline{w'^2\theta'_v}]$ are the main sinks of $\overline{w'^3}$, and they balance the buoyancy production $(3g/\theta_{vs})\overline{w'^2\theta'_v}$ and the turbulent advection $-(1/\rho_s)(\partial\overline{w'^4}/\partial z)$ [Eq. (B1)]. As the turbulent mixing time scale $\tau$ is small near the stably stratified layer, $-(C_8/\tau)\overline{w'^3}$ leads to a stronger damping that limits the growth of shallow convection and $\overline{w'^3}$ near the top of boundary layer. Because of the relatively large positive $\overline{w'^3}$, the Newtonian pressure damping dominates the $\overline{w'^3}$ budgets. A smaller C8 provides less restriction of $\overline{w'^3}$ and generates a larger skewness of vertical velocity

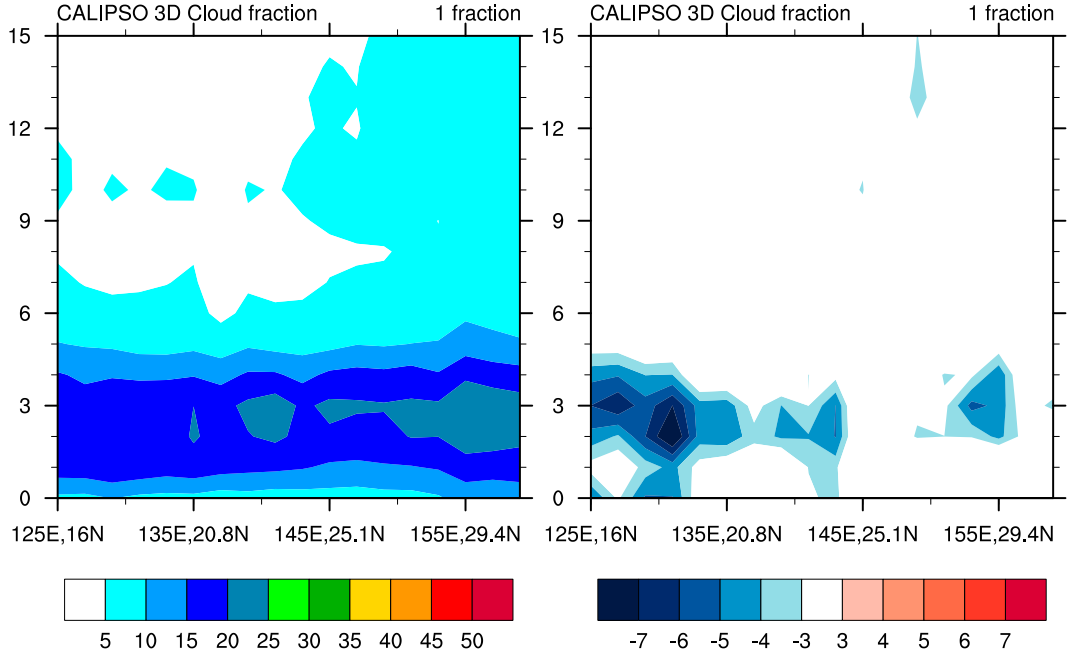


FIG. C1. Vertical cross sections of the meridionally averaged cloud fraction along the EAMS in DJFMAM (box in Fig. 1). (left) The climatological mean cloud fraction section, which is averaged from 2007 to 2017. (right) The anomalies of two El Niño years (2010, 2016).

$\overline{w'^3}/(\overline{w'^2})^{1.5}$ in a turbulent flow. It means that the subgrid updrafts are narrower and stronger, which are balanced by broader and weak downdrafts. The boundary layer becomes more convective and the stratiform cloud can more easily transit to shallow convection (less reflection). As a result, a stronger positive low cloud feedback should be expected. Conversely, a larger $C_8$ leads to a weaker positive (or even a negative) low cloud feedback. This is because the strong turbulent mixing driven by local warm SST would increase stratocumulus and enhance reflection in the case of weaker convective drying.

Therefore, in the PACE_Nino_STRFB run, we reduce $C_8$ from 4.2 to 2 in EAMS (Fig. 1e) for a stronger local low cloud feedback. It should be noted that we still use the default configuration outside the box of EAMS, in order to keep the cloud feedback and atmospheric circulations unchanged.

## APPENDIX C

### Cloud Fraction Changes Derived by *CALIPSO*

Figure C1 shows vertical cross sections of the meridionally averaged cloud fraction along the EAMS in DJFMAM (box in Fig. 1). Although the *CALIPSO* dataset has a short time span and contains only two El Niño events, the low cloud reduction is consistent with Figs. 1 and 2.

## REFERENCES


Bony, S., and J. L. Dufresne, 2005: Marine boundary layer clouds at the heart of tropical cloud feedback uncertainties in climate models. *Geophys. Res. Lett.*, **32**, L20806, https://doi.org/10.1029/2005GL023851.

——, K. M. Lau, and Y. C. Sud, 1997: Sea surface temperature and large-scale circulation influences on tropical greenhouse effect and cloud radiative forcing. *J. Climate*, **10**, 2055–2077, https://doi.org/10.1175/1520-0442(1997)010<2055:SSTALS>2.0.CO;2.

——, and Coauthors, 2006: How well do we understand and evaluate climate change feedback processes? *J. Climate*, **19**, 3445–3482, https://doi.org/10.1175/JCLI3819.1.

Bretherton, C. S., P. N. Blossey, and C. R. Jones, 2013: Mechanisms of marine low cloud sensitivity to idealized climate perturbations: A single-LES exploration extending the CGILS cases. *J. Adv. Model. Earth Syst.*, **5**, 316–337, https://doi.org/10.1002/jame.20019.

Ceppi, P., F. Brient, M. D. Zelinka, and D. L. Hartmann, 2017: Cloud feedback mechanisms and their representation in global climate models. *Wiley Interdiscip. Rev.: Climate Change*, **8**, e465, https://doi.org/10.1002/wcc.465.

Cess, R. D., M. Zhang, B. A. Wielicki, D. F. Young, X.-L. Zhou, and Y. Nikitenko, 2001: The influence of the 1998 El Niño upon cloud-radiative forcing over the Pacific warm pool. *J. Climate*, **14**, 2129–2137, https://doi.org/10.1175/1520-0442(2001)014<2129:TIOTEN>2.0.CO;2.

Clement, A. C., R. Burgman, and J. R. Norris, 2009: Observational and model evidence for positive low-level cloud feedback. *Science*, **325**, 460–464, https://doi.org/10.1126/science.1171255.

Danabasoglu, G., and Coauthors, 2020: The Community Earth System Model version 2 (CESM2). *J. Adv. Model. Earth Syst.*, **12**, e2019MS001916, https://doi.org/10.1029/2019MS001916.

Dee, D. P., and Coauthors, 2011: The ERA-Interim reanalysis: Configuration and performance of the data assimilation system. *Quart. J. Roy. Meteor. Soc.*, **137**, 553–597, https://doi.org/10.1002/qj.828.

Galperin, B., S. Sukoriansky, and P. S. Anderson, 2007: On the critical Richardson number in stably stratified turbulence. *Atmos. Sci. Lett.*, **8**, 65–69, https://doi.org/10.1002/asl.153.

Geoffroy, O., S. C. Sherwood, and D. Fuchs, 2017: On the role of the stratiform cloud scheme in the inter-model spread of cloud feedback. *J. Adv. Model. Earth Syst.*, **9**, 423–437, https://doi.org/10.1002/2016MS000846.

Golaz, J.-C., V. E. Larson, and W. R. Cotton, 2002: A PDF-based model for boundary layer clouds. Part I: Method and model description. *J. Atmos. Sci.*, **59**, 3540–3551, https://doi.org/10.1175/1520-0469(2002)059<3540:APBMFB>2.0.CO;2.

——, ——, J. A. Hansen, D. P. Schanen, and B. M. Griffin, 2007: Elucidating model inadequacies in a cloud parameterization by use of an ensemble-based calibration framework. *Mon. Wea. Rev.*, **135**, 4077–4096, https://doi.org/10.1175/2007MWR2008.1.

Guo, Z., and Coauthors, 2014: A sensitivity analysis of cloud properties to CLUBB parameters in the single-column Community Atmosphere Model (SCAM5). *J. Adv. Model. Earth Syst.*, **6**, 829–858, https://doi.org/10.1002/2014MS000315.

——, and Coauthors, 2015: Parametric behaviors of CLUBB in simulations of low clouds in the Community Atmosphere Model (CAM). *J. Adv. Model. Earth Syst.*, **7**, 1005–1025, https://doi.org/10.1002/2014MS000405.

Hartmann, D. L., and K. Larson, 2002: An important constraint on tropical cloud–climate feedback. *Geophy. Res. Lett.*, **29**, 1951, https://doi.org/10.1029/2002GL015835.

Holtslag, A. A. M., and B. A. Boville, 1993: Local versus nonlocal boundary-layer diffusion in a global climate model. *J. Climate*, **6**, 1825–1842, https://doi.org/10.1175/1520-0442(1993)006<1825:LVNBLD>2.0.CO;2.

Huang, B., Y. Xue, D. Zhang, A. Kumar, and M. J. McPhaden, 2010: The NCEP GODAS ocean analysis of the tropical Pacific mixed layer heat budget on seasonal to interannual time scales. *J. Climate*, **23**, 4901–4925, https://doi.org/10.1175/2010JCLI3373.1.

——, ——, H. Wang, W. Wang, and A. Kumar, 2012: Mixed layer heat budget of the El Niño in NCEP climate forecast system. *Climate Dyn.*, **39**, 365–381, https://doi.org/10.1007/s00382-011-1111-4.

Klein, S. A., and D. L. Hartmann, 1993: The seasonal cycle of low stratiform clouds. *J. Climate*, **6**, 1587–1606, https://doi.org/10.1175/1520-0442(1993)006<1587:TSCOLS>2.0.CO;2.

Larson, V. E., 2017: CLUBB-SILHS: A parameterization of subgrid variability in the atmosphere. arXiv, 1711.03675, https://doi.org/10.48550/arXiv.1711.03675.

——, and J.-C. Golaz, 2005: Using probability density functions to derive consistent closure relationships among higher-order moments. *Mon. Wea. Rev.*, **133**, 1023–1042, https://doi.org/10.1175/MWR2902.1.

——, ——, and W. R. Cotton, 2002: Small-scale and mesoscale variability in cloudy boundary layers: Joint probability density functions. *J. Atmos. Sci.*, **59**, 3519–3539, https://doi.org/10.1175/1520-0469(2002)059<3519:SSAMVI>2.0.CO;2.

——, D. P. Schanen, M. Wang, M. Ovchinnikov, and S. Ghan, 2012: PDF parameterization of boundary layer clouds in

models with horizontal grid spacings from 2 to 16 km. *Mon. Wea. Rev.*, **140**, 285–306, https://doi.org/10.1175/MWR-D-10-05059.1.

Li, J. D., W. C. Wang, X. Q. Dong, and J. Y. Mao, 2017: Cloud-radiation-precipitation associations over the Asian monsoon region: An observational analysis. *Climate Dyn.*, **49**, 3237–3255, https://doi.org/10.1007/s00382-016-3509-5.

Medeiros, B., B. Stevens, and S. Bony, 2015: Using aquaplanets to understand the robust responses of comprehensive climate models to forcing. *Climate Dyn.*, **44**, 1957–1977, https://doi.org/10.1007/s00382-014-2138-0.

Neggers, R. A. J., 2015: Attributing the behavior of low-level clouds in large-scale models to subgrid-scale parameterizations. *J. Adv. Model. Earth Syst.*, **7**, 2029–2043, https://doi.org/10.1002/2015MS000503.

Norris, J. R., 2000: Interannual and interdecadal variability in the storm track, cloudiness, and sea surface temperature over the summertime North Pacific. *J. Climate*, **13**, 422–430, https://doi.org/10.1175/1520-0442(2000)013<0422:IAIVIT>2.0.CO;2.

——, and C. B. Leovy, 1994: Interannual variability in stratiform cloudiness and sea surface temperature. *J. Climate*, **7**, 1915–1925, https://doi.org/10.1175/1520-0442(1994)007<1915:IVISCA>2.0.CO;2.

Rayner, N. A., D. E. Parker, E. B. Horton, C. K. Folland, L. V. Alexander, D. P. Rowell, E. C. Kent, and A. Kaplan, 2003: Global analyses of sea surface temperature, sea ice, and night marine air temperature since the late nineteenth century. *J. Geophys. Res.*, **108**, 4407, https://doi.org/10.1029/2002JD002670.

Rossow, W. B., and R. A. Schiffer, 1999: Advances in understanding clouds from ISCCP. *Bull. Amer. Meteor. Soc.*, **80**, 2261–2287, https://doi.org/10.1175/1520-0477(1999)080<2261:AIUCFI>2.0.CO;2.

Stubenrauch, C. J., and Coauthors, 2013: Assessment of global cloud datasets from satellites: Project and database initiated by the GEWEX radiation panel. *Bull. Amer. Meteor. Soc.*, **94**, 1031–1049, https://doi.org/10.1175/BAMS-D-12-00117.1.

Stuecker, M. F., F. F. Jin, A. Timmermann, and S. McGregor, 2015: Combination mode dynamics of the anomalous northwest Pacific anticyclone. *J. Climate*, **28**, 1093–1111, https://doi.org/10.1175/JCLI-D-14-00225.1.

Tan, Z., T. Schneider, J. Teixeira, and K. G. Pressel, 2016: Large-eddy simulation of subtropical cloud-topped boundary layers: 1. A forcing framework with closed surface energy balance. *J. Adv. Model. Earth Syst.*, **8**, 1565–1585, https://doi.org/10.1002/2016MS000655.

Wang, B., R. Wu, and X. Fu, 2000: Pacific–East Asian teleconnection: How does ENSO affect East Asian climate? *J. Climate*, **13**, 1517–1536, https://doi.org/10.1175/1520-0442(2000)013<1517:PEATHD>2.0.CO;2.

——, R. G. Wu, and T. Li, 2003: Atmosphere–warm ocean interaction and its impacts on Asian–Australian monsoon variation. *J. Climate*, **16**, 1195–1211, https://doi.org/10.1175/1520-0442(2003)16<1195:AOIAII>2.0.CO;2.

——, J. Li, and Q. He, 2017: Variable and robust East Asian monsoon rainfall response to El Niño over the past 60 years (1957–2016). *Adv. Atmos. Sci.*, **34**, 1235–1248, https://doi.org/10.1007/s00376-017-7016-3.

Wood, R., 2012: Stratocumulus clouds. *Mon. Wea. Rev.*, **140**, 2373–2423, https://doi.org/10.1175/MWR-D-11-00121.1.

Woodruff, S. D., H. F. Diaz, E. C. Kent, R. W. Reynolds, and S. J. Worley, 2008: The evolving SST record from ICOADS. *Climate Variability and Extremes During the Past 100 Years*, S. Brönnimann et al., Eds., Advances in Global Change Research, Vol. 33, Springer, 65–83, https://doi.org/10.1007/978-1-4020-6766-2_4.

Wu, B., T. Zhou, and T. Li, 2017a: Atmospheric dynamic and thermodynamic processes driving the western North Pacific anomalous anticyclone during El Niño. Part I: Maintenance mechanisms. *J. Climate*, **30**, 9621–9635, https://doi.org/10.1175/JCLI-D-16-0489.1.

——, ——, and ——, 2017b: Atmospheric dynamic and thermodynamic processes driving the western North Pacific anomalous anticyclone during El Niño. Part II: Formation processes. *J. Climate*, **30**, 9637–9650, https://doi.org/10.1175/JCLI-D-16-0495.1.

Xie, S.-P., and Coauthors, 2009: Indian Ocean capacitor effect on Indo-western Pacific climate during the summer following El Niño. *J. Climate*, **22**, 730–747, https://doi.org/10.1175/2008JCLI2544.1.

Yang, J., Q. Liu, S.-P. Xie, Z. Liu, and L. Wu, 2007: Impact of the Indian Ocean SST basin mode on the Asian summer monsoon. *Geophys. Res. Lett.*, **34**, L02708, https://doi.org/10.1029/2006GL028571.

Yu, L., and R. A. Weller, 2007: Objectively analyzed air–sea heat fluxes for the global ice-free oceans (1981–2005). *Bull. Amer. Meteor. Soc.*, **88**, 527–540, https://doi.org/10.1175/BAMS-88-4-527.

Yu, R., B. Wang, and T. Zhou, 2004: Climate effects of the deep continental stratus clouds generated by the Tibetan Plateau. *J. Climate*, **17**, 2702–2713, https://doi.org/10.1175/1520-0442(2004)017<2702:CEOTDC>2.0.CO;2.

Zhang, H., and Coauthors, 2018: Low-cloud feedback in CAM5-CLUBB: Physical mechanisms and parameter sensitivity analysis. *J. Adv. Model. Earth Syst.*, **10**, 2844–2864, https://doi.org/10.1029/2018MS001423.

Zhang, M., and Coauthors, 2013: CGILS: Results from the first phase of an international project to understand the physical mechanisms of low cloud feedbacks in single column models. *J. Adv. Model. Earth Syst.*, **5**, 826–842, https://doi.org/10.1002/2013MS000246.

Zhang, R., A. Sumi, and M. Kimoto, 1996: Impact of El Niño on the East Asian monsoon: A diagnostic study of the '86/87 and '91/92 events. *J. Meteor. Soc. Japan*, **74**, 49–62, https://doi.org/10.2151/jmsj1965.74.1_49.

Zhou, T., and Coauthors, 2016: GMMIP (v1.0) contribution to CMIP6: Global monsoons model inter-comparison project. *Geosci. Model Dev.*, **9**, 3589–3604, https://doi.org/10.5194/gmd-9-3589-2016.

Zhu, P., and Coauthors, 2005: Intercomparison and interpretation of single-column model simulations of a nocturnal stratocumulus-topped marine boundary layer. *Mon. Wea. Rev.*, **133**, 2741–2758, https://doi.org/10.1175/MWR2997.1.